# Bidirectional genome-wide CRISPR screens reveal host factors regulating SARS-CoV-2, MERS-CoV and seasonal HCoVs

Antoine Rebendenne, Priyanka Roy, Boris Bonaventure, Ana Luiza Chaves Valadão, Lowiese Desmarets, Mary Arnaud-Arnould, Yves Rouillé, Marine Tauziet, Donatella Giovannini, Jawida Touhami, et al.

ARTICLES
https://doi.org/10.1038/s41588-022-01110-2

nature genetics

Check for updates

# Bidirectional genome-wide CRISPR screens reveal host factors regulating SARS-CoV-2, MERS-CoV and seasonal HCoVs

Antoine Rebendenne[1], Priyanka Roy[2], Boris Bonaventure[1,10], Ana Luiza Chaves Valadão[1,10], Lowiese Desmarets[3], Mary Arnaud-Arnould[1], Yves Rouillé[3], Marine Tauziet[1], Donatella Giovannini[4,5], Jawida Touhami[4,6], Yenarae Lee[2], Peter DeWeirdt[2], Mudra Hegde[2], Serge Urbach[7], Khadija El Koulali[8], Francisco Garcia de Gracia[1], Joe McKellar[1], Jean Dubuisson[3], Mélanie Wencker[9], Sandrine Belouzard[3], Olivier Moncorgé[1], John G. Doench[2]✉ and Caroline Goujon[1]✉

**CRISPR knockout (KO) screens have identified host factors regulating severe acute respiratory syndrome coronavirus 2 (SARS-CoV-2) replication. Here, we conducted a meta-analysis of these screens, which showed a high level of cell-type specificity of the identified hits, highlighting the necessity of additional models to uncover the full landscape of host factors. Thus, we performed genome-wide KO and activation screens in Calu-3 lung cells and KO screens in Caco-2 colorectal cells, followed by secondary screens in four human cell lines. This revealed host-dependency factors, including AP1G1 adaptin and ATP8B1 flippase, as well as inhibitors, including mucins. Interestingly, some of the identified genes also modulate Middle East respiratory syndrome coronavirus (MERS-CoV) and seasonal human coronavirus (HCoV) (HCoV-NL63 and HCoV-229E) replication. Moreover, most genes had an impact on viral entry, with AP1G1 likely regulating TMPRSS2 activity at the plasma membrane. These results demonstrate the value of multiple cell models and perturbational modalities for understanding SARS-CoV-2 replication and provide a list of potential targets for therapeutic interventions.**

SARS-CoV-2 is the etiologic agent of the coronavirus disease 2019 (COVID-19) pandemic. SARS-CoV-2 is the third highly pathogenic coronavirus to cross the species barrier in the 21st century after SARS-CoV-1 in 2002–2003 (refs. [1–3]) and MERS-CoV in 2012 (ref. [4]). Four additional HCoVs (HCoV-229E, HCoV-NL63, HCoV-OC43 and HCoV-HKU1) are known to circulate seasonally in humans, contributing to approximately one-third of common cold infections[5]. Like SARS-CoV-1 and HCoV-NL63, SARS-CoV-2 entry into target cells is mediated by the angiotensin-converting enzyme 2 (ACE2) receptor[6–10]. The cellular serine protease transmembrane protease serine 2 (TMPRSS2) is used by both SARS-CoV-1 and SARS-CoV-2 for Spike protein priming at the plasma membrane[6,11]. Cathepsins are also involved in SARS-CoV spike protein cleavage and fusion peptide exposure upon entry via an endocytic route, in the absence of TMPRSS2 (refs. [12–15]).

Several whole-genome KO CRISPR screens for the identification of coronavirus regulators have been reported[16–21]. These screens used naturally permissive simian Vero E6 cells of kidney origin[20]; human Huh7 cells (or derivatives) of liver origin (ectopically expressing ACE2 and TMPRSS2, or not)[16,18,19]; and A549 cells of lung origin, ectopically expressing ACE2[17,21]. Here, we conducted genome-wide, loss-of-function CRISPR KO screens and gain-of-function CRISPRa screens in several cell lines, including physiologically relevant human Calu-3 cells and Caco-2 cells, of lung and colorectal adenocarcinoma origin, respectively, followed by secondary screens in these cell lines and in Huh7.5.1 and A549 cells. Well-known SARS-CoV-2 host-dependency factors were identified among top hits, such as ACE2 and either TMPRSS2 or cathepsin L (depending on the cell type). We characterized the mechanism of action of the top hits and assessed their effect on other coronaviruses and influenza A orthomyxovirus. Altogether, this study provides insights into the coronavirus life cycle by identifying host factors that modulate replication and might lead to pan-coronavirus strategies for host-directed therapies.

## Results

**Meta-analysis of CRISPR KO screens highlights the importance of multiple models.** Vero E6 cells present high levels of cytopathic effects (CPEs) upon SARS-CoV-2 replication, making them ideal to perform whole-genome CRISPR screens for host factor identification. A *Chlorocebus sabaeus* single-guide RNA (sgRNA) library was previously successfully used to identify host factors regulating SARS-CoV-2 (isolate USA-WA1/2020) replication[20]. Therefore, we initially repeated whole-genome CRISPR KO screens in Vero E6 cells using the SARS-CoV-2 isolate BetaCoV/France/IDF0372/2020 (Fig. 1a). Importantly, *ACE2* was a top hit (Fig. 1b

[1]IRIM, CNRS, Montpellier University, Montpellier, France. [2]Genetic Perturbation Platform, Broad Institute of MIT and Harvard, Cambridge, MA, USA. [3]Lille University, CNRS, INSERM, CHU Lille, Institut Pasteur de Lille, Lille, France. [4]IGMM, CNRS, Montpellier University, Montpellier, France. [5]Metafora Biosystems, Paris, France. [6]Laboratory of Excellence GR-Ex, Paris, France. [7]IGF, Montpellier University, CNRS, INSERM, Montpellier, France. [8]BCM, Montpellier University, CNRS, INSERM, Montpellier, France. [9]CIRI, INSERM, CNRS, ENS-Lyon, Lyon University, Lyon, France. [10]These authors contributed equally: Boris Bonaventure, Ana Luiza Chaves Valadão. ✉e-mail: jdoench@broadinstitute.org; caroline.goujon@irim.cnrs.fr

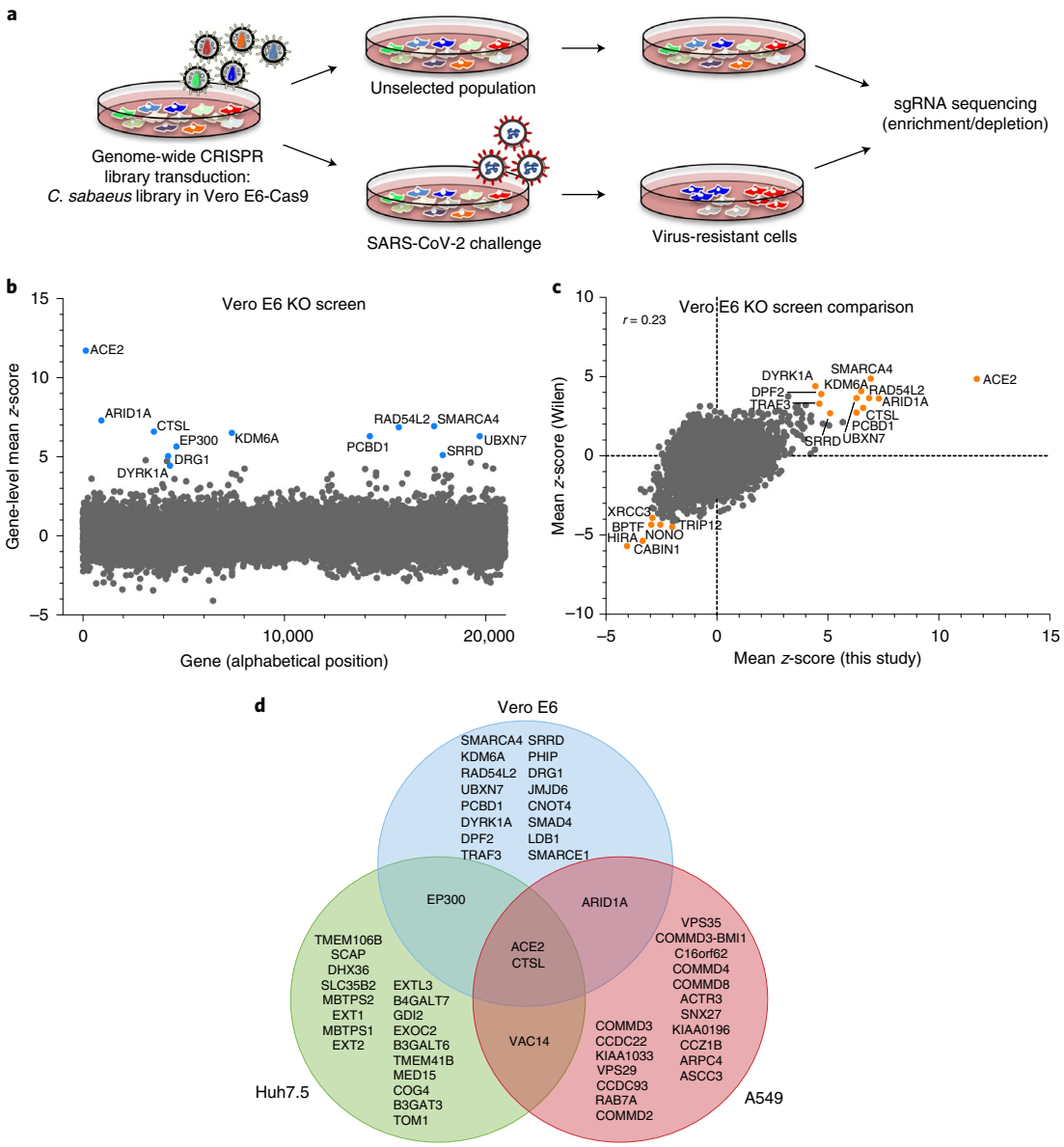


**Fig. 1 | Cell-type specificity of SARS-CoV-2 regulators identified by CRISPR screens. a**, Schematic of pooled screen pipeline to identify SARS-CoV-2 regulators in Vero E6 cells. **b**, Scatter plot showing the gene-level mean *z*-scores of genes when knocked out in Vero E6 cells. The top genes conferring resistance to SARS-CoV-2 are annotated and shown in blue ($n = 20{,}928$). **c**, Comparison between this Vero E6 screen to the Vero E6 screen conducted by the Wilen lab[20]. Genes that scored among the top 20 resistance hits and sensitization hits in both screens are labeled. Pearson's correlation coefficient *r* is indicated ($n = 20{,}928$). **d**, Venn diagram comparing hits across screens conducted in Vero E6, A549 and Huh7.5 (or Huh7.5.1) cells (ectopically expressing ACE2 and TMPRSS2 or not)[16–21]. The top 20 genes from each cell line are included, with genes considered a hit in another cell line if the average *z*-score was >3.

and Supplementary Data 1). Compared to prior results from the Wilen lab[20], this screen showed greater statistical significance for proviral (resistance) hits, suggesting that our screening conditions resulted in stronger selective pressure (Fig. 1c and Extended Data Fig. 1a,b). Nevertheless, proviral hits were consistent across the two screens, with 11 genes scoring in the top 20 of both datasets, including *ACE2* and *CTSL*; similarly, 6 of the top 20 antiviral (sensitization) hits were in common, including *HIRA* and *CABIN1*, both members of an H3.3-specific chaperone complex.

Additional genome-wide screens for SARS-CoV-2 host factors have varied in the viral isolate, CRISPR library and cell type (Supplementary Table 1)[16–21]. We reprocessed the data via the same analysis pipeline to enable fair comparisons (Methods and Supplementary Data 2); top-scoring genes were consistent with the analyses provided in the original publications. We next averaged gene-level *z*-scores and compared results across the Vero E6, A549 and Huh7.5 cell lines (Supplementary Note 1 and Fig. 1d). Overall, these analyses suggest that there is a strong cell-type specificity in the identified hits and that individual cell models are particularly suited, in as-yet unpredictable ways, to probe different aspects of SARS-CoV-2 host factor biology.

**Bidirectional screens identify genes regulating SARS-CoV-2 replication.** Calu-3 cells are a particularly attractive model for exploring SARS-CoV-2 biology, as they naturally express ACE2 and TMPRSS2, and we have previously shown that they behave

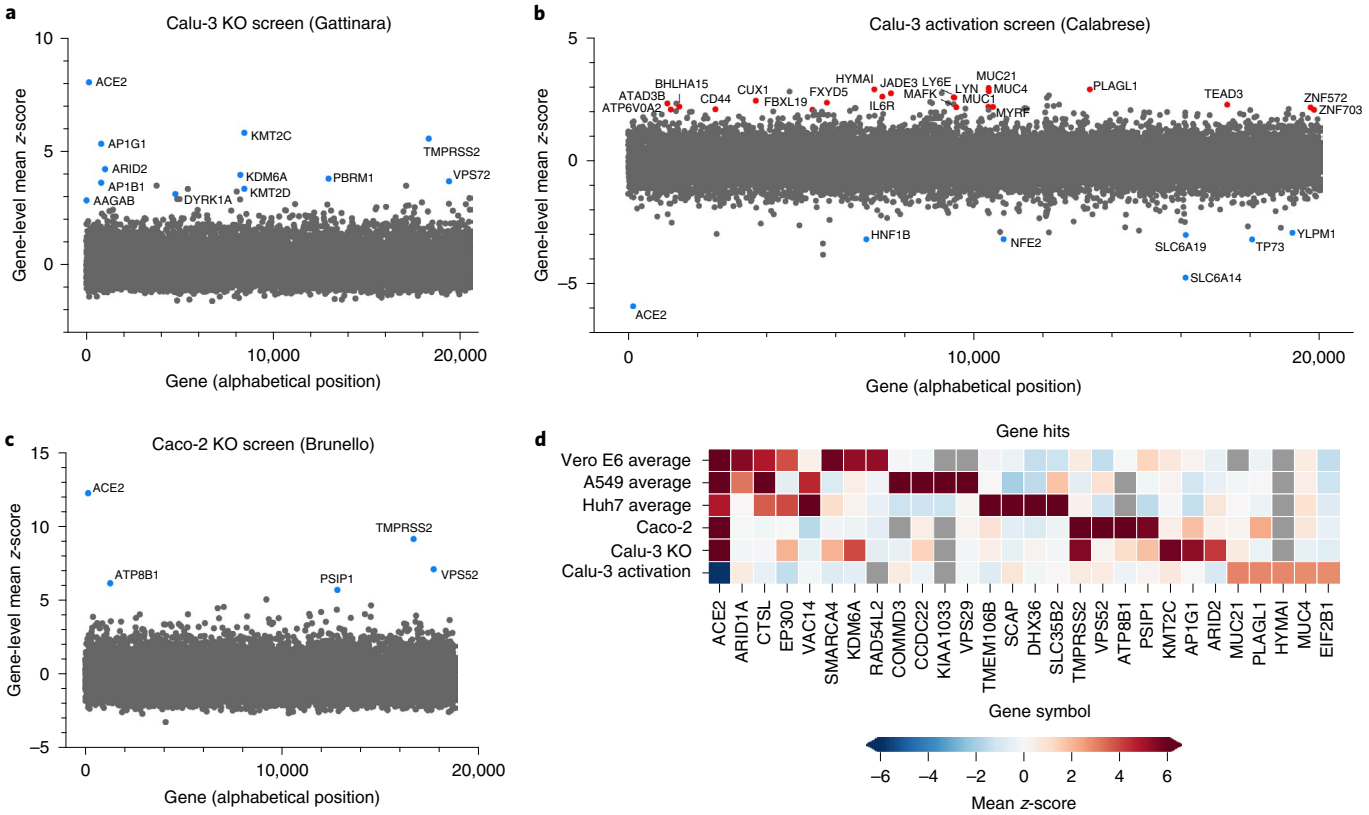


**Fig. 2 | Genome-wide CRISPR screens in Calu-3 reveal regulators of SARS-CoV-2. a**, Scatter plot showing the gene-level mean *z*-scores of genes when knocked out in Calu-3 cells. The top genes conferring resistance to SARS-CoV-2 are annotated and shown in blue. This screen did not have any sensitization hits ($n = 20{,}513$). **b**, Scatter plot showing the gene-level mean z-scores of genes when overexpressed in Calu-3 cells. The top genes conferring resistance and sensitivity to SARS-CoV-2 are annotated and shown in red and blue, respectively ($n = 20{,}000$). **c**, Scatter plot showing the gene-level mean z-scores of genes when knocked out in Caco-2 cells. The top genes conferring resistance to SARS-CoV-2 are annotated and shown in blue ($n = 18{,}804$). **d**, Heatmap of top five resistance hits from each cell line after averaging across screens in addition to genes that scored in multiple cell lines based on the criteria used to construct the Venn diagram in Fig. 1d (based on previous studies[16–21] and this study). Gray squares indicate genes that were filtered out for that particular cell line due to number of guides targeting that gene (Methods).

highly similarly to primary human airway epithelia (HAE) when challenged with SARS-CoV-2 (ref. [22]). Additionally, they are suited to viability-based screens, as they show high levels of CPEs upon SARS-CoV-2 replication, although their slow doubling time (~5–6 days) presents challenges for scale-up. The compact Gattinara library[23], known to perform as well as the larger Brunello library[20], was selected for the KO screen, whereas the Calabrese library[24] was used for the CRISPRa screen.

The KO screen was most powered to identify proviral factors (Extended Data Fig. 2a), and the top three genes were *ACE2*, *KMT2C* and *TMPRSS2* (Fig. 2a and Supplementary Data 3). Importantly, the latter did not score in any of the cell models discussed above[16–21]; conversely, *CTSL* did not score in this screen. Interestingly, whereas the BRG1/BRM-associated factor (BAF)-specific *ARID1A* scored in Vero E6 and A549 cells, Polybromo-associated BAF (PBAF)-specific components *ARID2* and *PRBM1* scored as top hits in Calu-3 cells. Additional new hits include *AP1G1*, *AP1B1* and *AAGAB*, which encode proteins that are part of, or regulate, the AP-1 complex. The latter is involved in the formation of clathrin-coated pits and vesicles and is important for vesicle-mediated, ligand–receptor complex intracellular trafficking.

In contrast to the KO screen, the CRISPRa screen detected both pro- and antiviral genes (Fig. 2b, Extended Data Fig. 2b and Supplementary Data 4). Reassuringly, the top-scoring proviral hit was *ACE2*. Several solute carrier transport channels also scored, including *SLC6A19*, a known partner of ACE2 (ref. [25]). On the antiviral side of the screen, a top scoring hit was *LY6E*, which is a known restriction factor of coronaviruses[26]. Additionally, *MUC21*, *MUC4* and *MUC1* all scored. Mucins are heavily glycosylated proteins and have a well-established role in host defense against pathogens[27,28]. Moreover, MUC4 has been recently proposed to possess a protective role against SARS-CoV-1 pathogenesis in a mouse model[29].

To expand the range of cell lines examined further, we also performed a KO screen with the Brunello library[20] in Caco-2 cells, which express *ACE2* but were engineered to overexpress it (hereafter named Caco-2-ACE2), to increase CPE levels and enable viability-based screening. Similar to Calu-3 cells, *ACE2* and *TMPRSS2* were the top resistance hits (Fig. 2c, Extended Data Fig. 2a,c and Supplementary Data 5), indicating that Caco-2 and Calu-3 cells, unlike previously used models, rely on TMPRSS2-mediated cell entry, rather than the endocytic pathway. Assembling all the proviral genes identified across five cell lines, we confirmed that screen results are largely cell line dependent (Fig. 2d). Finally, we directly compared the KO and activation screens conducted in Calu-3 cells (Extended Data Fig. 2d). The only gene that scored with both perturbation modalities was *ACE2*, emphasizing that different aspects of biology are revealed by these screening technologies.

**Hit identification is reproducible within cell line and technology in secondary screens.** To validate the genome-wide CRISPR results, we collated hit genes from both published screens and those

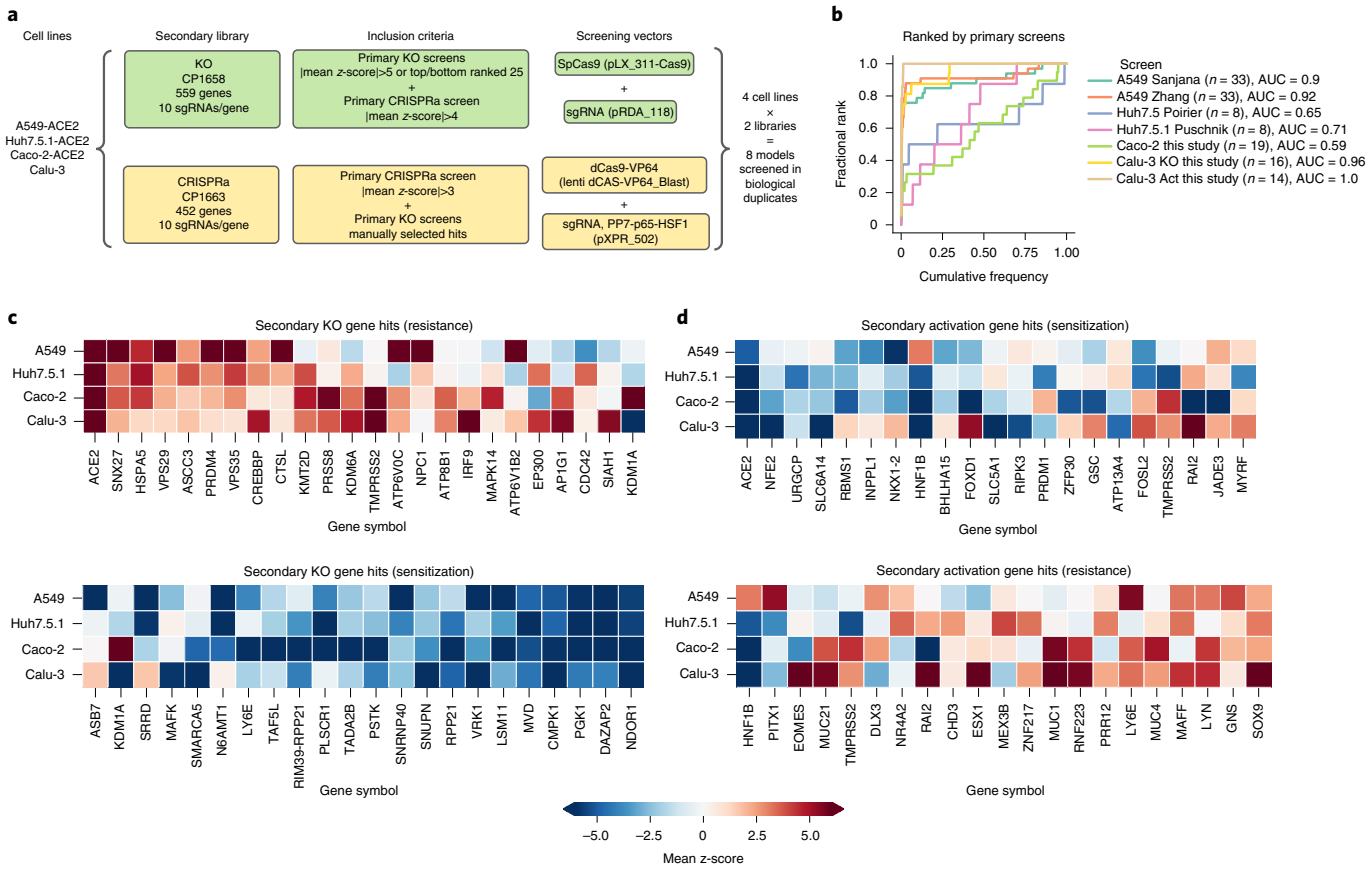


**Fig. 3 | Secondary screens in Calu-3, Caco-2-ACE2, A549-ACE2 and Huh7.5.1-ACE2 cells. a**, Schematic of secondary library design and screen strategy. **b**, Cumulative distribution plots analyzing overlap of top hits between primary and secondary screens. Putative hit genes from the primary screen are ranked by mean *z*-score, and classified as validated hits based on mean *z*-score in the secondary screen, using a threshold of greater than 3 for KO or less than −3 for activation. AUC, area under the curve. **c**, Heatmap comparison of top resistance and sensitization hits from secondary KO screens across cell lines. **d**, Heatmap comparison of top resistance and sensitization hits from secondary activation screens across cell lines.

presented here, including ten guides per gene and generating both KO and activation libraries (Fig. 3a and Supplementary Data 6–16). We then conducted two independent secondary screens in four human cell lines: Calu-3, Caco-2-ACE2, A549-ACE2 and Huh7.5.1-ACE2 cells. These secondary screens showed high replicate reproducibility (Extended Data Fig. 3a–d,e–h). Excellent concordance with their respective primary screens was observed for Calu-3 and A549-ACE2 cells, but a lower reproducibility was observed for Huh7.5.1 and Caco-2 cells (Fig. 3b). A detailed description of secondary screen data is provided in Supplementary Note 2.

Comparisons between KO and activation screens confirmed that hits were largely directionally-dependent (Extended Data Fig. 3i–l). The secondary screens validated that the differences observed across cell systems (Fig. 3c,d) are largely attributed to true biological differences in these systems rather than both known and unknown differences in the execution of the primary CRISPR screens. Finally, a Cas12a-based secondary screen in Calu-3 cells confirmed the identification of some hits, such as *AP1G1*, and showed a good correlation with Cas9-based screens (Extended Data Fig. 4 and Supplementary Data 12).

**Individual validations confirm the identification of new proviral genes.** Next, we focused on proviral genes identified in our whole-genome KO screens and selected 22 candidates among the top ones identified in the primary screens performed in Calu-3, Vero E6 and Caco-2 cells. We designed two sgRNAs per candidate and generated polyclonal KO Calu-3 cell populations. Two weeks after transduction, KO cell lines were challenged with SARS-CoV-2

**Fig. 4 | Impact of the identified proviral genes on coronaviruses SARS-CoV-2, HCoV-229E, HCoV-NL63 and MERS-CoV and orthomyxovirus influenza A.** Calu-3-Cas9 cells were stably transduced to express two different sgRNAs (g1 and g2) per indicated gene or non-targeting, control sgRNAs (CTRL g1, g2), and selected. **a**, Cells were infected with SARS-CoV-2 bearing the mNG reporter, and the infection efficiency was scored 48 h later by flow cytometry. The cell lines/screens in which the candidates were identified are indicated below the graph. **b**, Cells were infected with influenza A virus bearing the Nanoluciferase (NLuc) reporter and 10 h later, relative infection efficiency was measured by monitoring NLuc activity. **c**, Cells were infected with HCoV-NL63, and 5 days later, relative infection efficiency was determined using RT-qPCR. **d**, Cells were infected with HCoV-229E-Renilla, and 48–72 h later, relative infection efficiency was measured by monitoring Renilla activity. **e**,**f**, Cells were infected with MERS-CoV, and 16 h later, the percentage of infected cells was determined using anti-spike (e) or anti-dsRNA (f) immunofluorescence (IF) staining followed by microscopy analysis ($n = 10$ fields per condition). The mean and standard error of the mean (s.e.m.) of three or more independent experiments are shown (a–f; except in panel b for *ATP8B1* g2 and in panels e and f for *ATP8B1* g1, $n = 2$). Statistical significance was determined with one-way ANOVA with Dunnett's test (*$P < 0.05$, **$P < 0.01$, ***$P < 0.001$, ****$P < 0.0001$) (a–f). Exact numbers and *P* values are indicated in Supplementary Data 17. The red and dark red dashed lines represent 50% and 80% inhibition, respectively.

bearing the mNeonGreen (mNG) reporter[30] and the percentage of infected cells was scored by flow cytometry (Fig. 4a and Extended Data Fig. 5a,b). KO of around half the selected genes induced at least a 50% decrease in infection efficiency. Among them, *AP1G1* KO had an inhibitory effect as drastic as *ACE2* KO (>95% decrease in infection efficiency). Another gene coding an Adaptin family member, *AP1B1*, and a gene coding a known partner of the AP-1 complex, *AAGAB*, also had an important impact (~70–90% decrease in infection). Immunoblot analysis showed effective depletion of these Adaptins in KO cell populations (Extended Data Fig. 5c). As previously reported[31,32], *AAGAB* KO had an impact on both *AP1G1* and *AP1B1* expression levels; *AP1B1* KO impacted

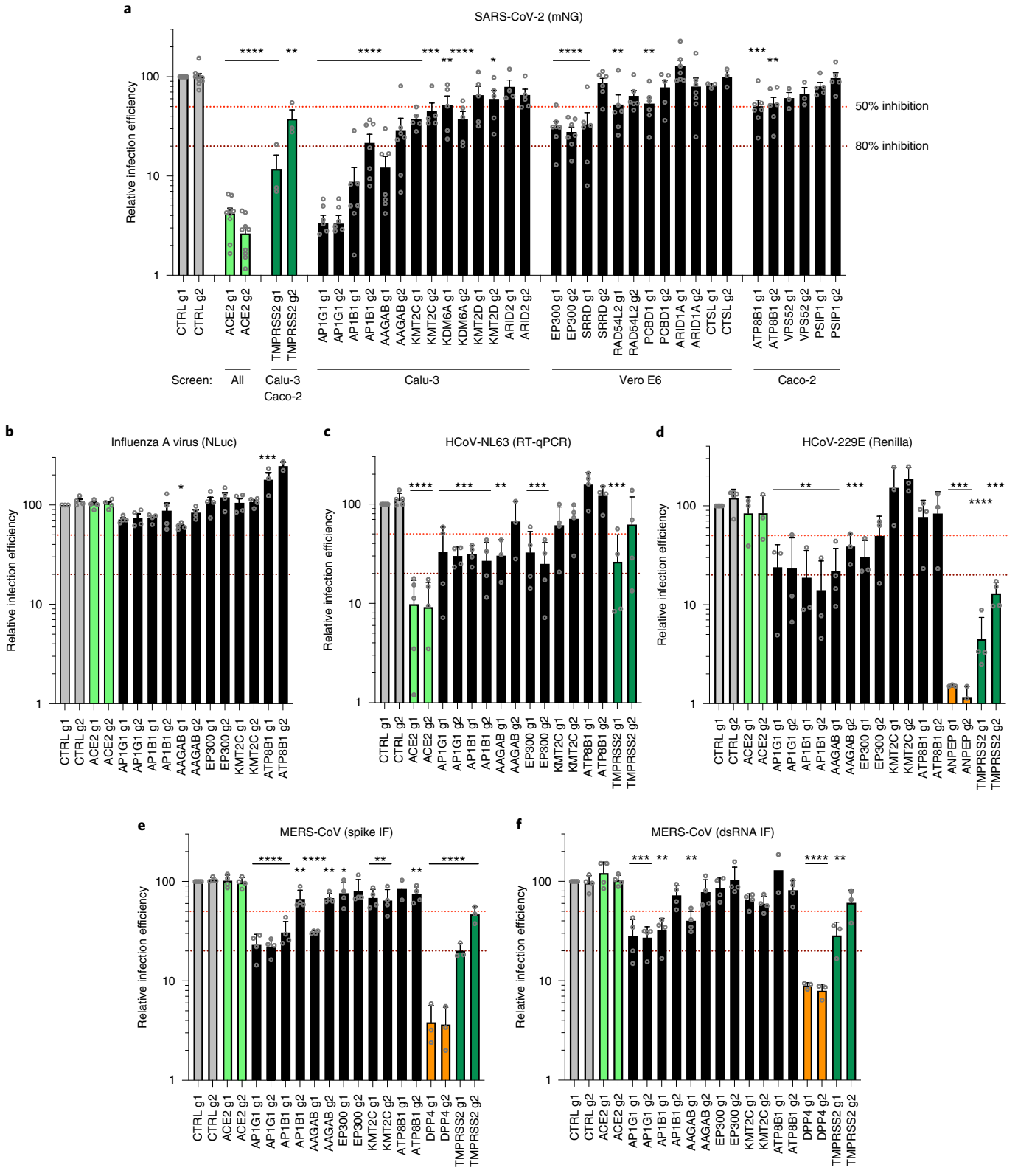

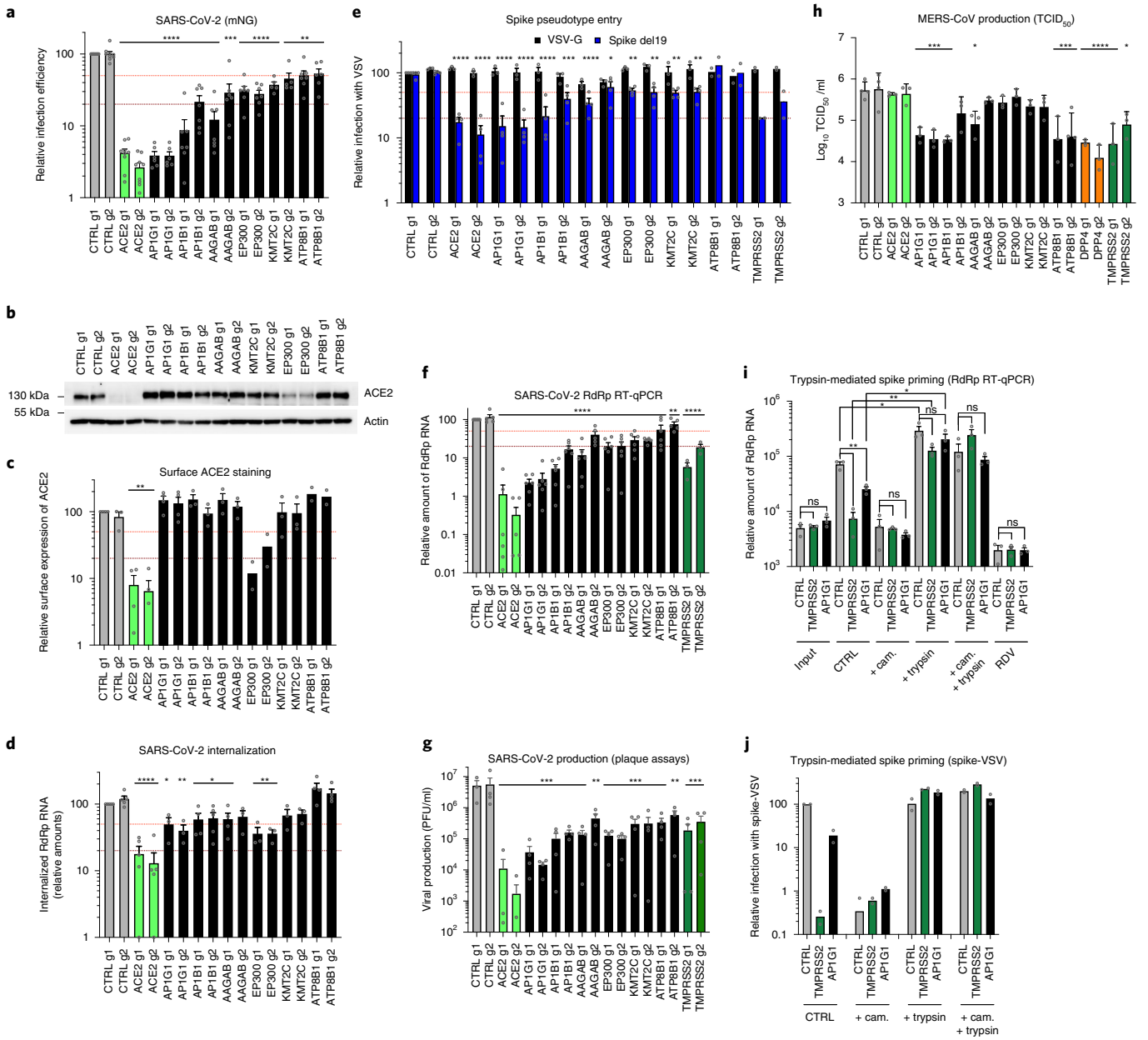


**Fig. 5 | Characterization of the impact of identified SARS-CoV-2 dependency factors.** Calu-3-Cas9 cells were transduced to express two sgRNAs (g1, g2) per gene or non-targeting, control sgRNAs (CTRL g1, g2). **a**, Cells were infected with SARS-CoV-2 mNG, and infection efficiency was scored 48 h later by flow cytometry. **b**, Expression levels of ACE2 were analyzed by immunoblot. Actin served as a loading control. A representative experiment (from two independent experiments) is shown. **c**, Relative surface ACE2 expression was measured using a Spike-RBD-mFc fusion followed by flow cytometry analysis. **d**, Cells were incubated with SARS-CoV-2 for 2 h, treated with Subtilisin A followed by RNA extraction and RdRp RT-qPCR analysis. **e**. Cells were infected with Spike del19 and VSV-G pseudotyped, GFP-expressing VSV, and infection efficiency was analyzed 24 h later by flow cytometry. **f**, Cells were infected with SARS-CoV-2 and, 24 h later, lysed for RNA extraction and RdRp RT-qPCR analysis. **g**, Supernatants from panel f were harvested and plaque assays performed. PFU, plaque-forming units. **h**, Cells were infected with MERS-CoV, and 16 h later, viral production in the supernatant was measured by the 50% tissue culture infectious dose ($TCID_{50}$). **i**, Cells were pretreated (or not) with camostat mesylate (cam.) or remdesivir (RDV), incubated with SARS-CoV-2 for 30 min on ice and washed. Spike was then primed with trypsin or not and the media replaced, and 7 h later, cells were lysed for RNA extraction and RdRp RT-qPCR analysis. **j**, Similar to panel i, with Spike-pseudotyped, Firefly-expressing VSV. Cells were lysed and relative infection measured by monitoring Firefly activity 24 h later. The mean and s.e.m. of five or more (a) or three or more (c–f,h,i; except for *EP300* and *ATP8B1* KO in panel c and for *ATP8B1* and *TMPRSS2* KO in panel e, $n=2$) or four (g) independent experiments, or the mean of two independent experiments (j), are shown. Statistical significance was analyzed using a two-sided *t* test with no adjustment for multiple comparisons (a,c,i) or a one-way ANOVA with Dunnett's test (d–h) (*$P<0.05$, **$P<0.01$, ***$P<0.001$, ****$P<0.0001$). Exact numbers and *P* values are indicated in Supplementary Data 17. The red and dark red dashed lines represent 50% and 80% inhibition, respectively (a,c–f).

*AP1G1* levels and vice versa (Extended Data Fig. 5c). The KO of three other genes, *KMT2C*, *EP300* and *ATP8B1*, which code for a lysine methyltransferase, a histone acetyl transferase and a flippase, respectively, inhibited the infection efficiency by at least 50%. The KO of the other tested genes in Calu-3 cells had little to no impact on SARS-CoV-2 replication (Fig. 4a and Extended Data Fig. 5b).

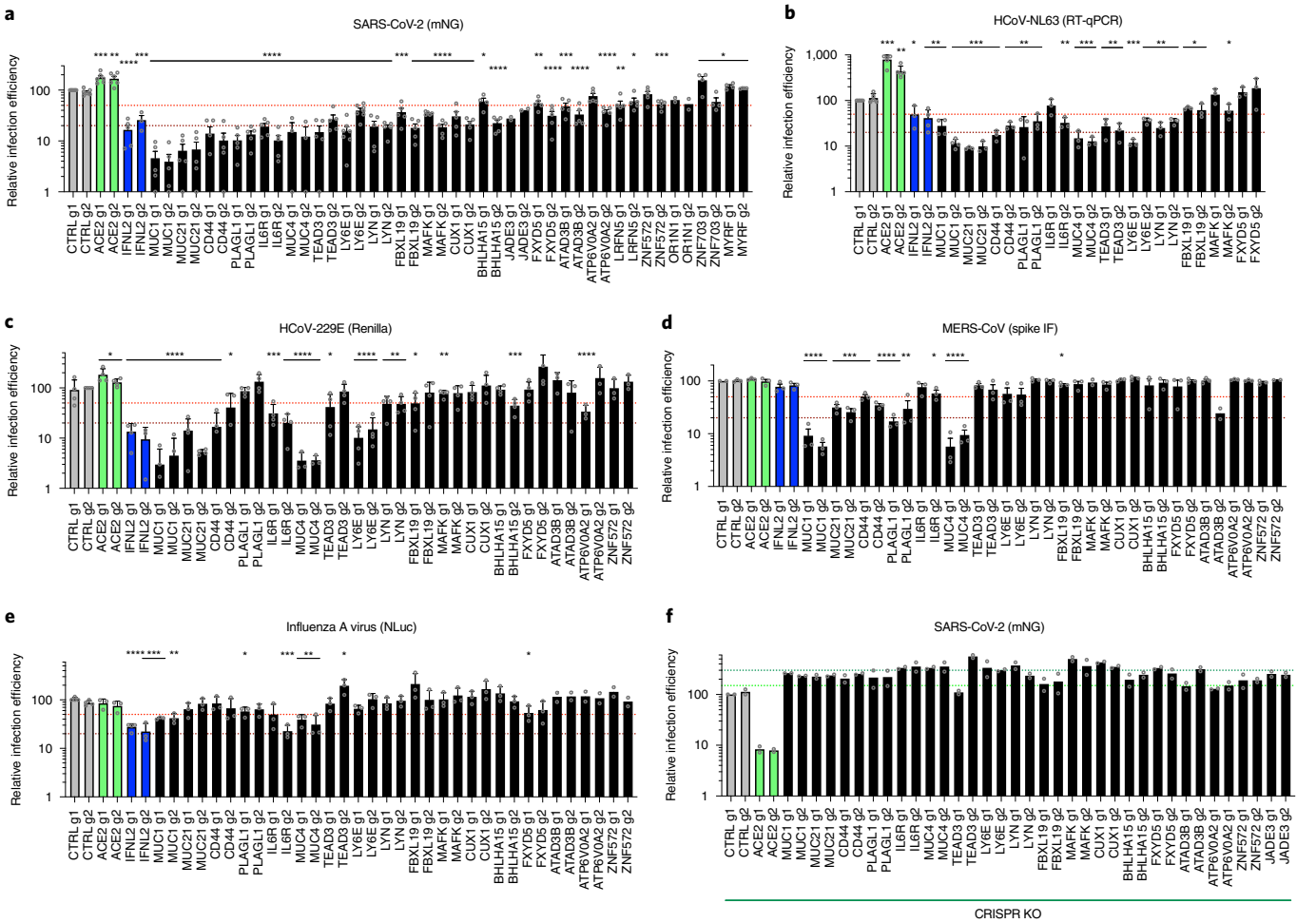


**Fig. 6 | Impact of the identified antiviral genes on coronaviruses SARS-CoV-2, HCoV-229E and MERS-CoV and orthomyxovirus influenza A.** Calu-3-dCas9-VP64 (a–e) or Calu-3-Cas9 (f) cells were stably transduced to express 2 sgRNAs (g1, g2) per indicated gene promoter (a–e) or coding region (f), or negative controls (CTRL) and selected for at least 10–15 days. **a**, Cells were infected with SARS-CoV-2 bearing the mNG reporter and the infection efficiency was scored 48 h later by flow cytometry. **b**, Cells were infected with HCoV-NL63, and infection efficiency was scored 5 days later by RT-qPCR. **c**, Cells were infected with HCoV-229E-Renilla, and 48–72 h later, relative infection efficiency was measured by monitoring Renilla activity. **d**, Cells were infected with MERS-CoV, and 16 h later, the percentage of infected cells was determined using anti-Spike IF staining followed by microscopy analysis ($n = 10$ fields per condition). **e**, Cells were infected with influenza A virus bearing the NLuc reporter, and 10 h later, relative infection efficiency was measured by monitoring NLuc activity. **f**, Cells were infected with SARS-CoV-2 bearing the mNG reporter, and the infection efficiency was scored 48 h later by flow cytometry. The mean and s.e.m. of three or more (a–e; except for panels a (*JADE3*, *OR1N1* KO), d (*MAFK1* g1, *ATAD3B* g2, *ZNF572* g2 KO) and e (*ATAD3B*, *ATP6V0A2*, *ZNF572* KO) $n = 2$) or two (f) independent experiments are shown. Statistical significance was determined by a two-sided *t*-test (*$P < 0.05$, **$P < 0.01$, ***$P < 0.001$, ****$P < 0.0001$) (**a**–**e**). Exact numbers and *P* values are indicated in Supplementary Data 17. The red and dark red dashed lines indicate 50% and 80% inhibition (a–e), and the green and dark green dashed lines indicate 150% and 300% increase in infection efficiency, respectively (f).

That a pooled screen can enrich for even a small fraction of cells harboring a KO, whereas this flow cytometry-based assay requires that a high-fraction of cells with a given guide manifest the phenotype, may explain these different outcomes, although we cannot rule out here poor KO efficiency in some cell populations. In parallel, the KO of these candidates on SARS-CoV-2-induced CPE (Extended Data Fig. 5d) mirrored the data obtained with the reporter virus, with the exception of *DYRK1A* KO (Fig. 5a and Extended Data Fig. 5b).

We then confirmed an important role of *AP1G1*, *AAGAB* and *ATP8B1* in Caco-2 cells (Extended Data Fig. 6a). However, *AP1B1* KO had little impact, but might have been insufficient (Extended Data Fig. 6a,d). *EP300* and *KMT2C* also played little or no role in these cells (Extended Data Fig. 6a), assuming their KO was efficient. None of the tested gene KOs inhibited replication in A549-ACE2 or Huh7.5.1-ACE2 cells (Extended Data Fig. 6b,c), despite a strong reduction of protein levels in KO populations (Extended Data Fig. 6e,f). Using RT-qPCR, we observed that the hits validated in Calu-3 cells (*AP1G1*, *AP1B1*, *AAGAB*, *KMT2C*, *EP300* and *ATP8B1*) were expressed at significantly higher levels in HAE compared to Calu-3 cells and to similar or higher levels in Caco-2 and A549-ACE2 cell lines (Extended Data Fig. 6g). Encouragingly, based on a recent single-cell RNA sequencing (scRNA-seq) study[33], these genes were all well expressed in SARS-CoV-2 primary target cells from the respiratory epithelia (Extended Data Fig. 6h).

Knocking out these candidate genes had no substantial impact on the replication of another respiratory virus, the orthomyxovirus influenza A virus (IAV), arguing against a general role in viral infection (Fig. 4b). In contrast, seasonal HCoV-NL63 replication was impacted by *AP1G1*, *AP1B1*, *AAGAB* (g1) and *EP300* KO, but not by *KMT2C* or *ATP8B1* KO (Fig. 4c). Interestingly, seasonal HCoV-229E and highly pathogenic MERS-CoV, which do not use ACE2

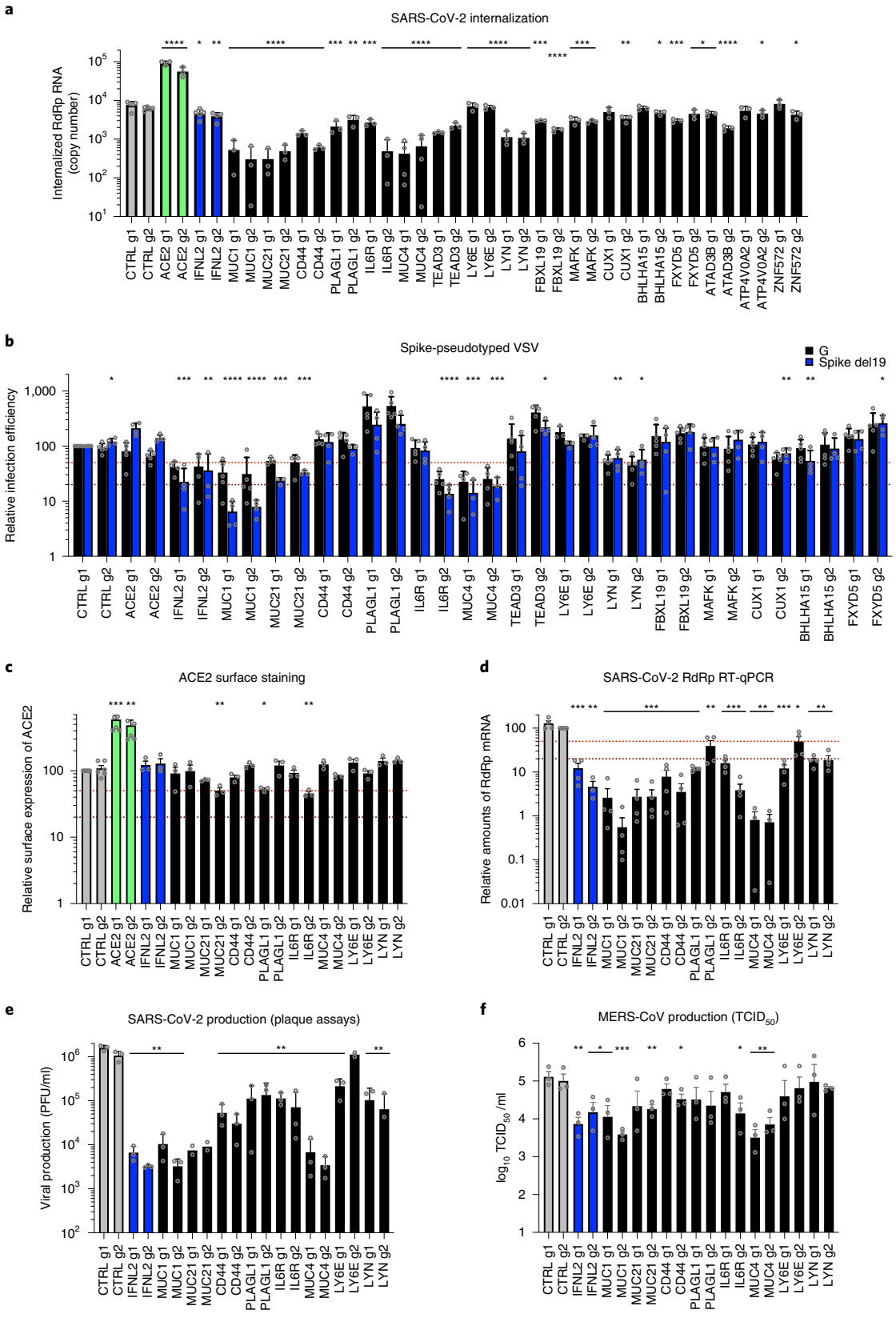


for entry but ANPEP and DPP4, respectively, were both strongly affected by *AP1G1*, and, to some extent, by *AP1B1* and *AAGAB* KO (Fig. 4d–f), showing a pan-coronavirus role of these genes.

Next, we aimed to determine the viral life cycle step affected by the best candidates, that is, with a >50% effect in mNG reporter expression (Fig. 5a). Immunoblot analysis revealed similar (or higher) expression levels of ACE2 in the different KO cell lines in comparison to controls, except for *ACE2* and *EP300* KO cells, which had decreased levels of ACE2 (Fig. 5b). Using a recombinant Spike receptor-binding domain (RBD) fused to a mouse Fc fragment

**Fig. 7 | Characterization of the impact of identified SARS-CoV-2 antiviral factors.** Calu-3-dCas9-VP64 cells were stably transduced to express two different sgRNAs (g1, g2) per indicated gene promoter and selected for 10–15 days. **a**, Cells were incubated with SARS-CoV-2 for 2 h and then treated with Subtilisin A followed by RNA extraction and RdRp RT-qPCR analysis. **b**, Cells were infected with Spike del19 and VSV-G pseudotyped, and Firefly-expressing VSV and infection efficiency was analyzed 24 h later by monitoring Firefly activity. **c**, Relative surface ACE2 expression was measured using a Spike-RBD-mFc fusion and a fluorescent secondary antibody followed by flow cytometry analysis. **d**, Cells were infected with SARS-CoV-2 and, 24 h later, lysed for RNA extraction and RdRp RT-qPCR analysis. **e**, Aliquots of the supernatants from panel d were harvested and plaque assays were performed to evaluate the production of infectious viruses in the different conditions. **f**, Cells were infected with MERS-CoV, and 16 h later, infectious particle production in the supernatant was measured by $TCID_{50}$. The mean and s.e.m. of three or more independent experiments are shown (a,c–f; except for panel e (*MUC21* and *LY6E* g2 KO), $n=2$). Statistical significance was determined by a two-sided *t* test with no adjustment for multiple comparisons (*$P<0.05$, **$P<0.01$, ***$P<0.001$, ****$P<0.0001$) (a–f). Exact numbers and *P* values are indicated in Supplementary Data 17. The red and the dark red (b–d) dashed lines represent 50% and 80% inhibition, respectively.

to stain ACE2 at the cell surface, no substantial decrease in ACE2 at the plasma membrane was observed, apart from *ACE2* and *EP300* KO cell lines, as expected (Fig. 5c). To assess the internalization efficiency of viral particles, we measured the relative amounts of internalized viruses (Fig. 5d). This showed that *AP1G1*, *AP1B1*, *AAGAB* and *EP300* KO impacted SARS-CoV-2 internalization to at least some extent, but not *ATP8B1* KO. We then used vesicular stomatitis virus (VSV) particles pseudotyped with either VSV-G glycoprotein or SARS-CoV-2 Spike, bearing a C-terminal deletion of 19 amino acids (hereafter named Spike del19) as a surrogate for viral entry[34,35] (Fig. 5e). Of note, both *ACE2* and *TMPRSS2* KO specifically impacted Spike del19-VSV infection, confirming that the pseudotypes mimicked wild-type SARS-CoV-2 entry in Calu-3 cells. Spike del19-dependent entry was affected in most cell lines in comparison to VSV-G-mediated entry, with, again, the exception of *ATP8B1* KO cells. Analysis of SARS-CoV-2 RNA replication by RdRp RT-qPCR (Fig. 5f) and viral production in the cell supernatants by plaque assays (Fig. 5g) mirrored the data obtained using the mNG reporter virus, apart from *ATP8B1* KO cells. Indeed, in the latter, there was only ~50% decrease in viral RNAs or mNG expression, but more than one order of magnitude reduction in viral production, pinpointing a late block during replication (Fig. 5a,f,g). *ATP8B1* KO also decreased infectious SARS-CoV-2 production in Caco-2 cells (Extended Data Fig. 6a, right panel) but had little to no impact in A549-ACE2 and Huh7.5.1-ACE2 cells (Extended Data Fig. 6b,c, right panels).

Importantly, similarly to SARS-CoV-2, MERS-CoV relied on AP1G1 and AP1B1 in Calu-3 cells, as *AP1G1* and *AP1B1* (g1) KO had an impact comparable to *DPP4* KO on viral production (Fig. 5h). Moreover, *ATP8B1* KO strongly impacted infectious MERS-CoV particle production, whereas it did not impact infection as measured by Spike or dsRNA intracellular staining (Figs. 5h and 4e,f), arguing for a common and late role of *ATP8B1* in the coronavirus replicative cycle.

We next investigated the adaptin role in viral replication. Our data showed that the KO of *AP1G1*, *AP1B1* or *AAGAB* specifically impacted SARS-CoV-2 infection with Spike del19-pseudotyped VSV (Fig. 5e), whereas it did not affect ACE2 expression at the cell surface (Fig. 5c). In line with this, the KO of these factors also impacted MERS-CoV and HCoV-229E, which use different receptors (Figs. 4d–f and 5h). However, all these coronaviruses may use TMPRSS2 for Spike priming at the plasma membrane[36–38]. Moreover, adaptin KO did not inhibit infection in cells in which entry occurs via the endosomal pathway (Extended Data Fig. 6b,c). Adaptins, which orchestrate polarized sorting at the trans-Golgi network and recycling endosomes[39], regulate surface levels of a high number of plasma membrane proteins[32]. Therefore, we hypothesized that they might be important for TMPRSS2 surface expression. To determine whether that was the case, we purified plasma membrane-associated proteins from control (CTRL), *TMPRSS2* and *AP1G1* KO cell populations but were unable to specifically detect endogenous TMPRSS2 by immunoblot using various commercial antibodies. We next used mass spectrometry analyses on plasma membrane extracts and total cell lysates from these Calu-3 KO cell populations but could not detect TMPRSS2 (Supplementary Data 18), which has been reported to be poorly abundant[40]. To indirectly address whether AP1G1 regulates TMPRSS2, we tested if *AP1G1* KO phenotype could be bypassed by exogenous priming of Spike (Fig. 5i). The viral input control showed no difference in virus binding among CTRL, *TMPRSS2* or *AP1G1* KO Calu-3 cells, and 7 h after infection, *TMPRSS2* and *AP1G1* KO showed decreased viral replication in comparison to CTRL KO, as expected. However, Spike priming with trypsin treatment rescued viral replication both in *TMPRSS2* KO and *AP1G1* KO cells. Similar results were obtained with SARS-CoV-2 mNG reporter (Extended Data Fig. 6i) and with Spike del19-pseudotyped VSV (Fig. 5j). Altogether, these data strongly suggested that AP1G1 regulates Spike priming, presumably in an indirect manner, by regulating TMPRSS2 levels at the plasma membrane.

**CRISPRa screen reveals genes regulating SARS-CoV-2 replication.** Next, 21 genes among the top-ranking hits conferring resistance to SARS-CoV-2 replication from the whole-genome CRISPRa

**Fig. 8 | Impact of the proviral genes identified by CRISPRa on coronaviruses SARS-CoV-2, HCoV-229E and HCoV-NL63 and orthomyxovirus influenza A.** Calu-3-dCas9-VP64 cells were stably transduced to express two different sgRNAs (g1, g2) per indicated gene promoter and selected. **a**, Cells were noninfected (N.I.) or incubated with SARS-CoV-2 bearing NLuc reporter, and the infection efficiency was scored 30 h later by monitoring NLuc activity. **b**, Cells were infected by SARS-CoV-2 at multiplicity of infection (m.o.i.) 0.05 and 5 days later stained with crystal violet. Representative images from two independent experiments are shown. **c**, Cells were infected with influenza A virus bearing NLuc reporter, and 10 h later, relative infection efficiency was measured by monitoring NLuc activity. **d**, Cells were infected with HCoV-NL63, and 5 days later, infection efficiency was determined using RT-qPCR. **e**, Cells were infected with HCoV-229E-Renilla, and 72 h later, relative infection efficiency was measured by monitoring Renilla activity. **f**, Cells were incubated with SARS-CoV-2 for 2 h and then treated with Subtilisin A followed by RNA extraction and RdRp RT-qPCR analysis as a measure of viral internalization. **g**, Cells were infected with Spike del19 and VSV-G pseudotyped, Firefly-expressing VSV and infection efficiency was analyzed 24 h later by monitoring Firefly activity. **h**, Cells were infected with SARS-CoV-2 and, 24 h later, lysed for RNA extraction and RdRp RT-qPCR analysis. **i**. Aliquots of the supernatants from panel h were harvested and plaque assays were performed to evaluate the production of infectious viruses in the different conditions. The mean and s.e.m. of three or more (a,c,e,f), four or more (d,g,h) or two (i) independent experiments are shown. Statistical significance was determined by a two-sided *t* test with (*$P<0.05$, **$P<0.01$, ***$P<0.001$, ****$P<0.0001$) (a,c–h). Exact numbers and *P* values are indicated in Supplementary Data 17. The green and dark green dashed lines indicate 150% and 300% increase in infection efficiency, respectively (a,c–e,g,h).

screens were selected for individual validation, using two sgRNAs in Calu-3-dCas9-VP64 cells. In parallel, non-targeting control sgRNAs (CTRL g1, g2) and sgRNAs targeting *ACE2* and *IFNL2* promoters were used as controls. The sgRNA-expressing cell lines were challenged with SARS-CoV-2 mNG reporter and the percentage of infected cells scored by flow cytometry (Fig. 6a). As expected[22,26,41], the induction of *IFNL2* and *LY6E* expression potently decreased SARS-CoV-2 replication. The increased expression of the vast majority of the selected hits induced at least a 50% decrease in infection efficiency, with at least one sgRNA. Some genes had a particularly potent impact on SARS-CoV-2 and decreased replication levels by 80% or more, including *MUC1*, *MUC21* and *MUC4*, as well as *CD44*, *PLAGL1*, *IL6R*, *TEAD3* and *LYN* (Fig. 6a). Additionally, published scRNA data[33] showed that most of the

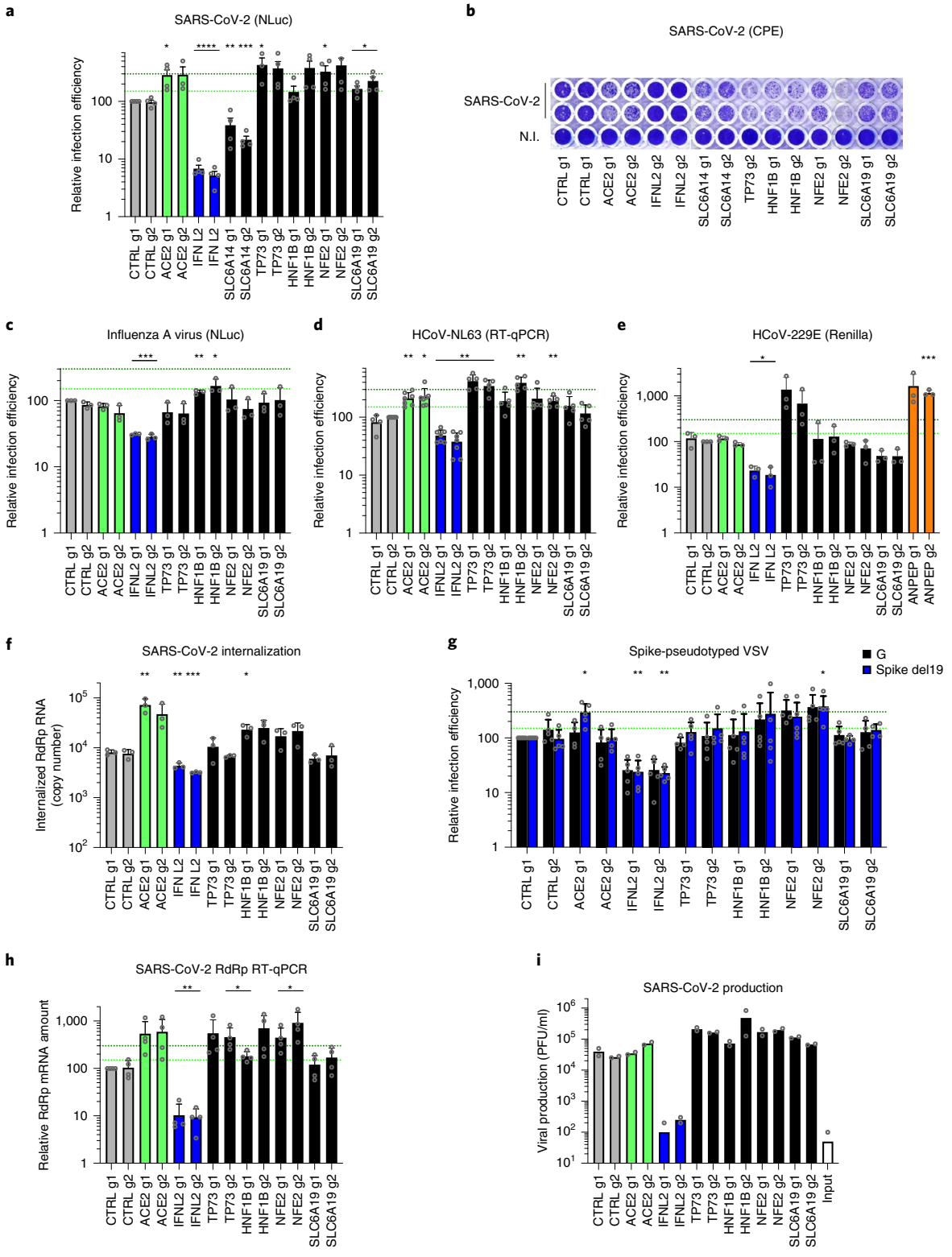

identified antiviral genes are expressed in a substantial percentage of airway epithelial cells (Extended Data Fig. 7a). Interestingly, primary HAE expressed *MUC1*, *MUC4*, *MUC21*, *IL6R*, *TEAD3* and *LYN* at significantly higher levels than Calu-3 cells whereas *CD44* was slightly less expressed) (Extended Data Fig. 7b). Expression levels in CRISPRa Calu-3 cells were relatively similar to those observed in HAE (Extended Data Fig. 7b,c). Moreover, *MUC21* was upregulated upon SARS-CoV-2 replication in HAE and Calu-3 cells, as well as *MUC4* in the latter (Extended Data Fig. 7d,e).

We then examined the antiviral breadth of some validated genes. HCoV-NL63 showed high sensitivity to increased expression of *MUC*s, *CD44*, *PLAGL1*, *TEAD3*, *LYN* or *LY6E* (Fig. 6b). Interestingly, similarly to SARS-CoV-2 and HCoV-NL63, HCoV-229E was highly sensitive to the overexpression of *MUC*s, *IL6R*, *LY6E* and *CD44*, but was less or not affected by the other genes, such as *PLAGL1* (Fig. 6c). MERS-CoV infection was impacted by overexpression of *MUC*s and to some extent by *PLAGL1*, *CD44*, *IL6R*, *LY6E* and *ATAD3B*, but not by the other genes (Fig. 6d). The induction of most candidate genes had no impact on IAV infection (Fig. 6e), with the exception of *MUC4* and *MUC1*, which decreased the infection efficiency by ~60–70%, as reported previously[28], and *IL6R*, with sgRNA g2 leading to 75% infection decrease. Finally, we assessed the impact of these antiviral genes by CRISPR KO and showed that the KO of most of them increased SARS-CoV-2 infection efficiency, confirming their physiological relevance (Fig. 6f).

Next, we tested several candidates in Caco-2 and in A549-ACE2 cells (Extended Data Fig. 8). *MUC4*, *MUC1* and *MUC21* overexpression potently decreased SARS-CoV-2 infection in these two cell lines. Moreover, *PLAGL1* also had a strong impact in A549-ACE2 cells, but not in Caco-2 cells, and the opposite was true for *LYN*. This might suggest a potential cell-type specificity for the former (e.g., lung origin) and possibly a dependence on ACE2/TMPRSS2 endogenous expression for the latter. *CD44* and *LY6E* also had some inhibitory effect in both cell lines. Taken together, these findings showed that the effect of the validated candidates could be observed in other cell types than Calu-3 cells, as also shown by the secondary screens (Fig. 3d).

Next, the SARS-CoV-2 internalization assay (performed as in Fig. 5d), showed that most of the validated genes, including those showing the strongest inhibitory phenotypes (namely *MUC1*, *MUC21*, *CD44*, *PLAGL1*, *IL6R*, *MUC4* and *LYN*) impacted viral internalization (Fig. 7a). The measure of viral entry using VSV pseudotypes globally mirrored the internalization data and showed that G-dependent entry was also sensitive to the overexpression of mucins, IL6R or LYN (Fig. 7b). However, whereas *CD44*, *PLAGL1* and *TEAD3* had an impact on SARS-CoV-2 entry as measured by the internalization assay, there was no effect of these genes on Spike del19-VSV pseudotype infection, perhaps highlighting subtle differences in the mechanism of entry between pseudotypes and wild-type SARS-CoV-2. Surprisingly, *LY6E* induction had no measurable impact on viral entry, using either the internalization assay or the pseudotypes, contrary to what was reported before[26]. Differences in the experimental systems used could explain the differences observed here and would require further investigation. ACE2 surface staining showed that inhibition of viral entry could not be explained by a decrease in ACE2 surface expression in most cases (Fig. 7c). Finally, the impact of the best candidates on SARS-CoV-2 and MERS-CoV replication, measured by RdRp RT-qPCR and plaque assays for SARS-CoV-2 (Fig. 7d,e) or $TCID_{50}$ for MERS-CoV (Fig. 7f), recapitulated what was observed with SARS-CoV-2 mNG reporter (Fig. 6a) and MERS-CoV Spike intracellular staining (Fig. 6d).

Noteworthy, the three mucins had the strongest impact on both SARS-CoV-2 and MERS-CoV production (~2 log and ~1 log decrease, respectively) (Fig. 7e,f). The activation of *IL6R*, *CD44*, *PLAGL1* and *LYN* also had a substantial impact on SARS-CoV-2 replication (~1 log decrease or more, for at least one sgRNA) but had a globally milder impact on MERS-CoV replication, with *LYN* having no impact at all (Fig. 7e,f). Whereas mucins are well known to act as antimicrobial barriers[42,43], the role of antiviral genes such as *IL6R*, *CD44* or *PLAGL1* in limiting SARS-CoV-2 entry remains to be elucidated.

Finally, in addition to the dependency factors identified by the KO screens, we selected several of the top-ranking hits conferring sensitization to SARS-CoV-2 replication in the CRISPRa screen (Fig. 8). We used the same type of approaches as previously and notably identified *TP73*, *NFE2* or *SLC6A19* as proviral genes, as described in Supplementary Note 3 (Fig. 8 and Extended Data Fig. 10).

## Discussion

Despite intense research efforts, much remains to be discovered about host factors regulating replication of SARS-CoV-2 and other coronaviruses. Recently, a number of whole-genome CRISPR KO screens successfully identified coronavirus host-dependency factors[16–21]. However, most of these screens relied on ACE2 ectopic expression and were performed in cells that do not express TMPRSS2, an important cofactor for entry[6] (with one exception[19]). Our meta-analysis of these screens revealed a high-level of cell-type specificity in the hits identified, indicating a need to pursue such efforts in other model cell lines, to better define the landscape of SARS-CoV-2 cofactors. We observed differential validation rates across cell lines, perhaps reflecting greater intrinsic heterogeneity of certain models and heightened sensitivity to exact experimental conditions[44].

Here, we performed bidirectional, genome-wide screens in physiologically relevant lung adenocarcinoma Calu-3 cells and KO screens in colorectal adenocarcinoma Caco-2 cells. We identified new host-dependency factors, which are essential for SARS-CoV-2 replication and other coronaviruses, namely MERS-CoV, HCoV-229E and HCoV-NL63. Furthermore, our study characterized new antiviral genes, some with potent and/or broad anti-coronavirus activity. Importantly, by using secondary libraries based on the hits retrieved from published screens and our screens and screening in four human cell lines (A549-ACE2, Calu-3, Caco-2-ACE2 and Huh7.5.1-ACE2), we further confirmed the reproducibility and strong cell-type specificity of the hits identified in viability-based whole-genome screens. These results emphasize the value of considering multiple cell models and perturbational modalities (both CRISPR KO and CRISPRa) to better unravel the full landscape of SARS-CoV-2 host factors.

Simultaneously with our screens, bidirectional, genome-wide screens were performed in Calu-3 cells by P. Hsu and colleagues[45]. Comparisons between our data and theirs showed good overlap in the hits identified (Extended Data Fig. 10), with shared hits including host-dependency factors adaptins AP1G1 and AP1B1, as well as the antiviral mucins. This comparison emphasizes the reproducibility of CRISPR screens conducted across different labs, even when different libraries are used, while further highlighting that the cellular model is the primary source of variability.

Most of the identified genes impacted the early phases of the replication cycle. This observation was true for both the host-dependency factors and the antiviral inhibitors, presumably emphasizing the fact that viral entry is the most critical step of the viral life cycle and probably, as such, the most easily targeted by natural defenses. Among the host-dependency factors essential for viral entry, the Adaptin AP1G1 and, to a lower extent, Adaptin AP1B1 and their partner AAGAB, surprisingly played a crucial role. The AP-1 complex regulates polarized sorting at the trans-Golgi network and/or recycling endosomes, and may play an indirect role in apical sorting[39]. Interestingly, AAGAB binds to and stabilizes AP1G1 (ref. [31]) and, as observed in our study, in *AAGAB* KO cells,

AP1G1 is less abundant[31], which may suggest a role of AAGAB via the regulation of AP-1 complex here. Our data showed that *AP1G1*, *AP1B1* and *AAGAB* are crucial host-dependency factors in Calu-3 cells for all coronaviruses studied here. More precisely, the KO of *AP1G1*, *AP1B1* or *AAGAB* impacted SARS-CoV-2 entry and this could be abrogated by exogenous (trypsin-mediated) priming of SARS-CoV-2 Spike. This suggested that the adaptins are important regulators of Spike priming, presumably indirectly, via the regulation of TMPRSS2. Further work will be necessary to fully elucidate the role of the adaptins in coronavirus entry and to determine whether they are necessary for the proper expression and/or localization of TMPRSS2 at the plasma membrane.

The only proviral gene acting at a late stage of the viral life cycle was ATP8B1, which belongs to the P4-type subfamily of ATPases transporters and is a flippase translocating phospholipids from the outer to the inner leaflet of membrane bilayers[46]. ATP8B1 is essential for proper apical membrane structure and mutations of this gene have been linked to cholestasis. The fact that ATP8B1 was important for both SARS-CoV-2 and MERS-CoV replication highlighted a potentially conserved role for coronaviruses. Interestingly, ATP8B1 and its homologous ATP8B2 were recently identified as binding-partners of SARS-CoV-2 ORF3 and M, respectively[47], suggesting that the virus might subvert their functions. Of note, TMEM41B, an integral protein of the endoplasmic reticulum known to regulate the formation of autophagosomes, lipid droplets and lipoproteins, was recently shown to be both an essential coronavirus cofactor[18] and a phospholipid scramblase whose deficiency impaired the normal cellular distribution of cholesterol and phosphatidylserine[48]. Whether ATP8B1 could play a similar role in coronavirus replication remains to be determined.

Among the best antivirals we identified through our CRISPRa screens, the well-known antimicrobial defenses, membrane-associated mucins played a broad and potent role at limiting coronavirus entry. Interestingly, these mucins were upregulated in COVID-19 patients[33]. In the context of influenza A virus infection[28,42], mucins were proposed to trap viruses before they can access to their receptors, which would be consistent with the effect we observed on viral entry here.

In conclusion, our study revealed a network of SARS-CoV-2 and other coronavirus regulators in model cell lines physiologically expressing ACE2 and TMPRSS2. Importantly, the main natural targets of SARS-CoV-2 in the respiratory tract co-express ACE2 and TMPRSS2, which highlight the importance of the models used here. Further characterization work on this newly identified landscape of coronavirus regulators may guide future therapeutic intervention.

## Online content

Any methods, additional references, Nature Research reporting summaries, source data, extended data, supplementary information, acknowledgements, peer review information; details of author contributions and competing interests; and statements of data and code availability are available at https://doi.org/10.1038/s41588-022-01110-2.

Received: 23 May 2021; Accepted: 26 May 2022;
Published online: 25 July 2022

## References

1. Drosten, C. et al. Identification of a novel coronavirus in patients with severe acute respiratory syndrome. *N. Engl. J. Med.* **348**, 1967–1976 (2003).
2. Peiris, J. et al. Coronavirus as a possible cause of severe acute respiratory syndrome. *Lancet* **361**, 1319–1325 (2003).
3. Zhong, N. et al. Epidemiology and cause of severe acute respiratory syndrome (SARS) in Guangdong, People's Republic of China, in February, 2003. *Lancet* **362**, 1353–1358 (2003).
4. Zaki, A. M., van Boheemen, S., Bestebroer, T. M., Osterhaus, A. D. M. E. & Fouchier, R. A. M. Isolation of a novel coronavirus from a man with pneumonia in Saudi Arabia. *N. Engl. J. Med.* **367**, 1814–1820 (2012).
5. van der Hoek, L. Human coronaviruses: what do they cause? *Antivir. Ther. (Lond.)* **12**, 651–658 (2007).
6. Hoffmann, M. et al. SARS-CoV-2 cell entry depends on ACE2 and TMPRSS2 and is blocked by a clinically proven protease inhibitor. *Cell* **181**, 271–280.e8 (2020).
7. Hofmann, H. et al. Human coronavirus NL63 employs the severe acute respiratory syndrome coronavirus receptor for cellular entry. *Proc. Natl. Acad. Sci. USA* **102**, 7988–7993 (2005).
8. Li, W. et al. Angiotensin-converting enzyme 2 is a functional receptor for the SARS coronavirus. *Nature* **426**, 450–454 (2003).
9. Wu, K., Li, W., Peng, G. & Li, F. Crystal structure of NL63 respiratory coronavirus receptor-binding domain complexed with its human receptor. *Proc. Natl Acad. Sci. USA* **106**, 19970–19974 (2009).
10. Zhou, P. et al. A pneumonia outbreak associated with a new coronavirus of probable bat origin. *Nature* **579**, 270–273 (2020).
11. Matsuyama, S. et al. Efficient activation of the severe acute respiratory syndrome coronavirus spike protein by the transmembrane protease TMPRSS2. *J. Virol.* **84**, 12658–12664 (2010).
12. Huang, I.-C. et al. SARS coronavirus, but not human coronavirus NL63, utilizes cathepsin L to infect ACE2-expressing cells. *J. Biol. Chem.* **281**, 3198–3203 (2006).
13. Ou, X. et al. Characterization of spike glycoprotein of SARS-CoV-2 on virus entry and its immune cross-reactivity with SARS-CoV. *Nat. Commun.* **11**, 1620 (2020).
14. Simmons, G. et al. Inhibitors of cathepsin L prevent severe acute respiratory syndrome coronavirus entry. *Proc. Natl Acad. Sci. USA* **102**, 11876–11881 (2005).
15. Koch, J. et al. TMPRSS2 expression dictates the entry route used by SARS-CoV-2 to infect host cells. *EMBO J.* **40**, e107821 (2021).
16. Baggen, J. et al. Genome-wide CRISPR screening identifies TMEM106B as a proviral host factor for SARS-CoV-2. *Nat. Genet.* https://doi.org/10.1038/s41588-021-00805-2 (2021).
17. Daniloski, Z. et al. Identification of required host factors for SARS-CoV-2 infection in human cells. *Cell* **184**, 92–105.e16 (2021).
18. Schneider, W. M. et al. Genome-scale identification of SARS-CoV-2 and pan-coronavirus host factor networks. *Cell* **184**, 120–132.e14 (2021).
19. Wang, R. et al. Genetic screens identify host factors for SARS-CoV-2 and common cold coronaviruses. *Cell* **184**, 106–119.e14 (2021).
20. Wei, J. et al. Genome-wide CRISPR screens reveal host factors critical for SARS-CoV-2 infection. *Cell* **184**, 76–91.e13 (2021).
21. Zhu, Y. et al. A genome-wide CRISPR screen identifies host factors that regulate SARS-CoV-2 entry. *Nat. Commun.* **12**, 961 (2021).
22. Rebendenne, A. et al. SARS-CoV-2 triggers an MDA-5-dependent interferon response which is unable to control replication in lung epithelial cells. *J Virol* https://doi.org/10.1128/JVI.02415-20 (2021).
23. DeWeirdt, P. C. et al. Genetic screens in isogenic mammalian cell lines without single cell cloning. *Nat. Commun.* **11**, 752 (2020).
24. Sanson, K. R. et al. Optimized libraries for CRISPR-Cas9 genetic screens with multiple modalities. *Nat. Commun.* **9**, 5416 (2018).
25. Camargo, S. M. R., Vuille-Dit-Bille, R. N., Meier, C. F. & Verrey, F. ACE2 and gut amino acid transport. *Clin. Sci. (Lond)* **134**, 2823–2833 (2020).
26. Pfaender, S. et al. LY6E impairs coronavirus fusion and confers immune control of viral disease. *Nat. Microbiol.* **5**, 1330–1339 (2020).
27. Chatterjee, M., van Putten, J. P. M. & Strijbis, K. Defensive properties of mucin glycoproteins during respiratory infections: relevance for SARS-CoV-2. *mBio* **11**, e02374-20 (2020).
28. McAuley, J. L. et al. The cell surface mucin MUC1 limits the severity of influenza A virus infection. *Mucosal Immunol.* **10**, 1581–1593 (2017).
29. Plante, J. A. et al. Mucin 4 protects female mice from coronavirus pathogenesis. Preprint at *bioRxiv* https://doi.org/10.1101/2020.02.19.957118 (2020).
30. Xie, X. et al. An infectious cDNA clone of SARS-CoV-2. *Cell Host Microbe* **27**, 841–848.e3 (2020).
31. Gulbranson, D. R. et al. AAGAB controls AP2 adaptor assembly in clathrin-mediated endocytosis. *Dev. Cell* **50**, 436–446.e5 (2019).
32. Wan, C. et al. AAGAB is an assembly chaperone regulating AP1 and AP2 clathrin adaptors. *J. Cell Sci.* https://doi.org/10.1242/jcs.258587 (2021).
33. Chua, R. L. et al. COVID-19 severity correlates with airway epithelium–immune cell interactions identified by single-cell analysis. *Nat. Biotechnol.* **38**, 970–979 (2020).
34. Rentsch, M. B. & Zimmer, G. A vesicular stomatitis virus Replicon-Based Bioassay for the Rapid and Sensitive Determination of Multi-Species Type I Interferon. *PLoS One* **6**, e25858 (2011).
35. Schmidt, F. et al. Measuring SARS-CoV-2 neutralizing antibody activity using pseudotyped and chimeric viruses. *J. Exp. Med.* **217**, e20201181 (2020).

36. Kawase, M., Shirato, K., van der Hoek, L., Taguchi, F. & Matsuyama, S. Simultaneous treatment of human bronchial epithelial cells with serine and cysteine protease inhibitors prevents severe acute respiratory syndrome coronavirus entry. *J. Virol.* **86**, 6537–6545 (2012).
37. Bertram, S. et al. TMPRSS2 activates the human coronavirus 229E for cathepsin-independent host cell entry and is expressed in viral target cells in the respiratory epithelium. *J Virol.* **87**, 6150–6160 (2013).
38. Gierer, S. et al. The spike protein of the emerging betacoronavirus EMC uses a novel coronavirus receptor for entry, can be activated by TMPRSS2, and is targeted by neutralizing antibodies. *J. Virol.* **87**, 5502–5511 (2013).
39. Nakatsu, F., Hase, K. & Ohno, H. The Role of the Clathrin Adaptor AP-1: Polarized Sorting and Beyond. *Membranes (Basel)* **4**, 747–763 (2014).
40. Saccon, E. et al. Cell-type-resolved quantitative proteomics map of interferon response against SARS-CoV-2. *iScience* **24**, 102420 (2021).
41. Stanifer, M. L. et al. Critical Role of Type III Interferon in Controlling SARS-CoV-2 Infection in Human Intestinal Epithelial Cells. *Cell Rep.* **7,** 32(1):107863 (2020).
42. Dhar, P. & McAuley, J. The role of the cell surface mucin MUC1 as a barrier to infection and regulator of inflammation. *Front. Cell. Infect. Microbiol.* **9**, 117 (2019).
43. Linden, S. K., Sutton, P., Karlsson, N. G., Korolik, V. & McGuckin, M. A. Mucins in the mucosal barrier to infection. *Mucosal Immunol.* **1**, 183–197 (2008).
44. Ben-David, U. et al. Genetic and transcriptional evolution alters cancer cell line drug response. *Nature* **560**, 325–330 (2018).
45. Biering, S. B. et al. Genome-wide, bidirectional CRISPR screens identify mucins as critical host factors modulating SARS-CoV-2 infection. Preprint at *bioRxiv* https://doi.org/10.1101/2021.04.22.4408488 (2021).
46. Paulusma, C. C. & Oude Elferink, R. P. J. The type 4 subfamily of P-type ATPases, putative aminophospholipid translocases with a role in human disease. *Biochim. Biophys. Acta* **1741**, 11–24 (2005).
47. Stukalov, A. et al. Multilevel proteomics reveals host perturbations by SARS-CoV-2 and SARS-CoV.*Nature* **594**, 246–252 (2021).
48. Li, Y. E. et al. TMEM41B and VMP1 are scramblases and regulate the distribution of cholesterol and phosphatidylserine. *J. Cell Biol.* **220**, e202103105 (2021).

## Methods

**Plasmids and constructs.** The pLX_311-Cas9 (Addgene, 96924), pRDA_174 (Addgene, 136476), pXPR_BRD109 (lenti dCAS-VP64_Blast[49], Addgene, 61425), which express Cas9, Cas12a and dCas9-VP64, respectively, have been described[24,50]. LentiGuide-Puro vector was a gift from F. Zhang[51,52] (Addgene, 52963), pRDA_118 is a modified version of this vector, with minor modifications to tracrRNA (Addgene, 133459), we have described before LentiGuide-Puro-CTRL g1 and g2 (ref. [53]) (Addgene, 139455, 139456). pXPR_502 vector for sgRNA expression for CRISPRa was also described[24] (Addgene, 96923). Guide RNA coding oligonucleotides were annealed and ligated into BsmBI-digested LentiGuide-Puro or pXPR_502 vectors, as described (Addgene); see Supplementary Table 2 for the sgRNA coding sequences used. pcDNA3.1_spike_del19 was a gift from R. De Francesco (Addgene, 155297). Our lentiviral vector expressing ACE2 (pRRL.sin.cPPT.SFFV/ACE2; Addgene, 145842) has been described previously[22].

**CRISPR libraries.** The human Gattinara, Brunello and *C. sabaeus* whole-genome KO libraries have been described[20,23,24] as has the human CRISPRa library Calabrese[24].

The Cas9-based KO secondary library included genes from each primary KO screen (this study and previous studies[16–21]) that either scored with a mean *z*-score greater than 5 or less than −5 or scored in the top or bottom 25 of the screen, as well as genes that scored with a mean *z*-score greater than 4 or less than −4 in the Calu-3 activation screen (Supplementary Data 6). The secondary KO library (CP1658) targets 559 genes, with a total of 6,084 sgRNA constructs, including 500 intergenic controls and an average of ten guides per gene. The sgRNAs were cloned into pRDA_118 (Addgene, 133459).

The CRISPRa secondary library included genes that scored with a mean *z*-score greater than 3 or less than −3 in the primary Calu-3 activation screen, as well as manually selected hits from the primary KO screens (Supplementary Data 7). The secondary CRISPRa library (CP1663) targets 452 genes, with a total of 5,001 sgRNA constructs, including 500 intergenic controls and an average of ten guides per gene. The sgRNAs were cloned into pXPR_502 (Addgene, 96923).

A custom secondary Cas12a-CRISPR KO library (CP1660) was designed with a total of 2,736 sgRNA constructs with four guides per gene (with two guides per gene on each construct) (Supplementary Data 6). A total of 500 intergenic control sites targeted by 250 constructs with two guides per construct were also included. The sgRNAs were cloned into pRDA_052 (Addgene, 136474).

**Cell lines.** Human Calu-3, Caco-2, HEK293T, A549, Huh7 and Huh7.5.1, simian Vero E6 and LLC-MK2, dog MDCK cells were maintained in complete Dulbecco's modified Eagle medium (DMEM) (Gibco) supplemented with 10% fetal bovine serum and penicillin/streptomycin. The following cell lines were obtained from American Type Culture Collection (ATCC): human Caco-2 (ATCC, HTB-37), Calu-3 (ATCC, HTB-55), HEK293T (ATCC, CRL-3216), A549 (ATCC, CCL-185; a gift from W. Barclay), simian LLC-MK2 cells (ATCC, CCL7.1; a gift from N. Arhel) and dog MDCK cells (ATCC, CCL-34; a gift from W. Barclay); simian Vero E6 cells were obtained from Sigma-Aldrich (reference 85020206; a gift from C. Chable-Bessia); Huh7 and Huh7.5.1 cells have been described previously[54,55] (and the latter provided by R. Gaudin). All cell lines were regularly screened for the absence of mycoplasma contamination using Lonza MycoAlert detection kit.

A549 and Huh7.5.1 cells (as well as Caco-2 cells, for the primary and secondary CRISPR screens) stably overexpressing ACE2 were generated by transduction with RRL.sin.cPPT.SFFV.ACE2.WPRE lentiviral vector[22].

For CRISPR-Cas9-mediated gene disruption, Calu-3, Caco-2(-ACE2), A549-ACE2 and Huh7.5.1-ACE2 cells stably expressing Cas9 or dCas9-VP64 were first generated by transduction with LX_311-Cas9 or XPR_BRD109, respectively, followed by blasticidin selection. Wild-type Cas9 activity was checked using the XPR_047 assay (a gift from D. Root, Addgene, 107145) and was always >80% (Supplementary Fig. 1a). dCas9-VP64 activity was checked using the pXPR_502 vector expressing sgRNA targeting IFITM3 and MX1 promoters (Supplementary Fig. 1b,c). Cells were transduced with guide RNA expressing LentiGuide-Puro or XPR_502 (as indicated) or the secondary libraries (CP1658 or CP1663, see above) and selected with antibiotics for at least 10 days.

For CRISPR-Cas12a-mediated gene disruption, Calu-3 cells stably expressing Cas12a were generated by transduction with RDA_174 and selected and then transduced with the CP1660 library and selected.

**Lentiviral production and transduction.** Lentiviral vector stocks were obtained by polyethylenimine (PEI) or Lipofectamine 3000 (Thermo Fisher Scientific)-mediated multiple transfections of 293T cells with vectors expressing Gag-Pol, the miniviral genome, the Env glycoprotein at a ratio of 1:1:0.5. The culture medium was changed 6 h after transfection, and vector containing supernatants harvested 36 h later, filtered and used directly or stored at −80 °C. Transduction was performed by cell incubation with the LV in the presence of polybrene (4 μg ml$^{-1}$) for a few hours. When necessary, spin infection was performed for 2 h at 30 °C and 1,000 *g* to improve transduction efficiencies. Antibiotics were added 24–48 h after transduction.

**Whole-genome and secondary CRISPR KO screens.** Vero E6, Caco-2-ACE2, Calu-3, A549-ACE2 and Huh7.5.1-ACE2 cells were transduced with LX_311-Cas9 lentiviral vector at a high m.o.i. and selected.

For the whole-genome screens, cells were grown to at least 120 million cells (40–60 million for Calu-3 cells) and transduced with lentiviral vectors coding the *C. sabaeus* sgRNAs[20] (for Vero E6), the Brunello library[24] (for Caco-2-ACE2) or the Gattinara library[23] (for Calu-3), at m.o.i. ~0.3–0.5. Transduced cells were selected and reamplified (for 10–15 days; that is, to at least the starting amounts) before SARS-CoV-2 challenge at m.o.i. 0.005. The day of the viral challenge, 40 million cells were harvested, pelleted by centrifugation and frozen down for subsequent genomic DNA (gDNA) extraction. Massive CPEs were observed 3–5 days after SARS-CoV-2 infection and cells were kept in culture for 11–13, 18–27 and 30–34 days in total before harvest and gDNA extraction, for Vero E6, Caco-2-ACE2 and Calu-3, respectively. The primary screens were performed in biological replicates (that is, with independently generated KO cell populations), as follows: the screens in Vero E6 cells were performed in biological duplicates, the first of which was then further divided into three technical replicates (that is, independent screens performed with the same KO population); the screens in Calu-3 cells were performed in biological quadruplicates, and the screens in Caco-2 cells in biological duplicates.

For the secondary CRISPR KO screens, 120 million Cas12a-expressing Calu-3 cells or 120 million Cas9-expressing Calu-3, Caco-2-ACE2, A549-ACE2 and Huh7.5.1-ACE2 were transduced with our CRISPR KO secondary library (CP1658 for Cas9, and CP1660 for Cas12a) at a low m.o.i. as above. Then, 10–15 days later, 40 million cells were either challenged with SARS-CoV-2 (m.o.i. 0.005) or harvested and frozen down for subsequent gDNA extraction. CPEs were observed 3–5 days after SARS-CoV-2 infection and cells were kept in culture for 8–11 days or 13–15 days for Cas9 and Cas12a-based screens, respectively, before gDNA extraction. Each secondary screen was performed in independent biological duplicates, with the exception of the Cas12a screen for which one replicate could not be analyzed due to poor sequencing quality.

**Whole-genome and secondary CRISPRa screens.** Calu-3, Caco-2-ACE2, A549-ACE2 and Huh7.5.1 cells were transduced with dCas9-VP64 (pXPR_BRD109)-expressing lentiviral vectors at a high m.o.i. and selected.

For the whole-genome CRISPRa screens, 120 million Calu-3-dCas9-VP64 cells were transduced with the Calabrese library[24] in two biological replicates (for sublibrary A) or in one replicate (for sublibrary B) at a low m.o.i. (~0.3–0.5). Then, 2.5 weeks later, 40 million cells were either challenged with SARS-CoV-2 (m.o.i. 0.005) or harvested and frozen down for subsequent gDNA extraction. CPEs were observed 3–5 days after SARS-CoV-2 infection and cells were kept in culture for 11–17 days before gDNA extraction.

For the secondary CRISPRa screens, 120 million dCas9-VP64-expressing Calu-3, Caco-2-ACE2, A549-ACE2 and Huh7.5.1-ACE2 were transduced with our CRISPRa secondary library (CP1658) and the screens were performed in the same conditions as above, with CPEs 3–5 days after infection and cells kept in culture for 10–13 days before gDNA extraction. Each secondary screen was performed in independent biological duplicates.

**gDNA preparation and sequencing.** gDNA was isolated using the QIAamp DNA Blood Maxi kit (Qiagen) or the NucleoSpin Blood XL kit (Macherey-Nagel), as per the manufacturer's instructions. Isolated gDNAs were cleaned up using the OneStep PCR Inhibitor Removal Kit (Zymo Research, D6030). PCR products were amplified using Titanium Taq polymerase (Takara) and purified using Agencourt AMPure XP SPRI beads (Beckman Coulter, A63880). Samples were sequenced on a HiSeq2500 HighOutput (Illumina) with a 5% spike-in of PhiX (Supplementary Note 4).

**Screen analysis.** For each published screen, the corresponding authors provided raw read counts. For the screens conducted in this paper, guide-level read counts were retrieved from sequencing data. We log-normalized read counts using the following formula:

$$\log - \text{normalized reads per million for guide} = \log_2\left(\frac{\text{number of reads per guide}}{\text{total reads in condition} \times 10^6} + 1\right).$$

When applicable, we averaged lognorm values across conditions (Poirier, Daelemans and Sanjana). We calculated log-fold changes for each condition relative to plasmid DNA (pDNA) lognorm values. If pDNA reads were not provided for the given screen, pDNA reads from a different screen that used the same library were used (Puschnik analysis used Sanjana pDNA; Zhang analysis used Poirier pDNA). For each condition in each data set, we fit a natural cubic spline between the control and infected conditions[20]. The degrees of freedom for each spline were fit using tenfold cross-validation. We calculated residuals from this spline and *z*-scored these values at the guide level, assuming a normal distribution; *P* values were calculated based on a two-tailed hypothesis test (anchors package; https://github.com/gpp-rnd/anchors). False discovery rate (FDR) values were calculated using the Benjamini–Hochberg method. Genes were filtered by number of guides per gene, which was generally one guide fewer or greater than the median number of genes per gene for that library (for example for Brunello screens, which has a median of 4 guides per gene, we applied a filter of 3 to 5 guides per gene). This

guide-filtering step accounts for any missing values in the file compiling data across all screens (Supplementary Data 2 and 6–7), We calculated gene-level z-scores by averaging across guides and conditions, and *P* values were combined across conditions using Fisher's method. We then used these filtered gene-level *z*-scores to rank the genes such that the gene ranked 1 corresponded to the top proviral hit. The files containing the read counts and gene-level residual *z*-scores for each screen have been deposited on Gene Expression Omnibus (primary screens: GSE175666; Supplementary Data 1–5) (secondary screens: GSE193834; Supplementary Data 6–16). All correlations were calculated using the Python package scipy.

Cumulative distribution plots were generated as explained in Supplementary Note 5.

**Wild-type and reporter SARS-CoV-2 production and infection.** Wild-type BetaCoV/France/IDF0372/2020 was supplied by S. van der Werf and the National Reference Centre for Respiratory Viruses (Institut Pasteur, Paris, France). The patient sample from which this virus was isolated was provided by X. Lescure and Y. Yazdanpanah from Bichat Hospital (Paris, France). The mNG[30] and NLuc[56] reporter SARS-CoV-2 were based on 2019-nCoV/USA_WA1/2020 isolated from the first reported case in the United States and provided through World Reference Center for Emerging Viruses and Arboviruses and University of Texas Medical Branch (UTMB) investigator P. Yong Shi.

Wild-type, mNG and NLuc SARS-CoV-2 were amplified in Vero E6 cells (m.o.i. 0.005) in serum-free media; supernatants were harvested at 48–72 h after infection when CPEs were observed and cleared by centrifugation, and aliquots were frozen down at −80 °C. Viral supernatants were titrated by plaque assays in Vero E6 cells. Typical titers were $3x10^6$–$3x10^7$ plaque-forming units per milliliter. Genome sequences of our viral stocks were verified through deep sequencing (Eurofins).

Simian and human cell infections were performed at the indicated m.o.i. (calculated from titers in Vero E6 cells) in serum-free DMEM and 5% serum-containing DMEM, respectively. The viral input was left for the duration of the experiment, unless specified otherwise. Viral supernatants were frozen down at −80 °C before titration by plaque assays on Vero E6 cells. Cells were trypsinized and percentage of cells expressing mNG scored by flow cytometry (NovoCyte, ACEA Biosciences) after fixation in PBS1X-2% paraformaldehyde (PFA), or cells were lysed in Passive Lysis buffer and NLuc activity measured using an Envision plate reader (Perkin-Elmer) or lysed in RLT buffer (Qiagen) followed by RNA extraction and RT-qPCR analysis, at the indicated time after infection.

**Seasonal coronavirus production and infection.** HCoV-229E-Renilla was a gift from V. Thiel[57] and amplified for 5–7 days at 33 °C in Huh7.5.1 cells, in 5% FCS-containing DMEM. HCoV-NL63 NR-470 was obtained through BEI Resources (National Institute of Allergy and Infectious Diseases, National Institutes of Health (NIAID, NIH)) and amplified for 5–7 days at 33 °C in LLC-MK2 simian cells, in 2% FCS-containing DMEM. Viral stocks were harvested when cells showed >50% CPEs. Viruses were titrated through $TCID_{50}$ and typical titers were $1.8x10^9$ $TCID_{50}$ $ml^{-1}$ and $10^6$ $TCID_{50}$ $ml^{-1}$ for HCoV-229E-Renilla and HCoV-NL63, respectively. Infections of Calu-3 were performed at m.o.i. 300 for HCoV-229E-Renilla (as measured on Huh7.5.1 cells) and m.o.i. 0.1 for HCoV-NL63 (as measured on LLC-MK2 cells), and infection efficiency was analyzed 2–3 days later by measuring Renilla activity (HCoV-229E-Renilla) or 5 days later by RT-qPCR (HCoV-NL63).

**MERS-CoV production and infection.** HEK293T cells were transfected with a bacmid containing a full-length cDNA clone of MERS-CoV (a king gift from L. Enjuanes[58]) and overlaid 6 h later with Huh7 cells. After lysis of Huh7 cells, cell supernatants were collected and the virus was further amplified on Huh7 cells. Viral stocks were aliquoted, frozen down and titrated by the $TCID_{50}$ method.

Calu-3 cells, seeded on glass coverslips (immunofluorescence) or in 48-well plates (infectivity titrations), were inoculated with MERS-CoV at an m.o.i. of 0.3. Sixteen hours after inoculation, supernatants were collected and stored at −80 °C. Coverslips were fixed with 3% PFA, permeabilized (0.4% Triton X-100) and blocked with 5% goat serum (GS) in PBS1X. Cells were labeled with a mixture of J2 antibody (Scicons; 1:400) and an anti-spike antibody (Sino Biological; 1:500), and then incubated with Alexa-488-conjugated donkey anti-mouse IgG and Alexa594-conjugated goat anti-rabbit IgG secondary antibodies (Jackson Immunoresearch; 1:400) in 5% GS in PBS supplemented with 1 µg $ml^{-1}$ DAPI (4′,6-diamidino-2-phenylindole). Coverslips were mounted on microscope slides in Mowiol 4-88-containing medium. Images were acquired on an Evos M5000 imaging system (Thermo Fisher Scientific) with a ×10 objective. For infectivity titrations, Huh7 cells, seeded in 96-well plates, were incubated with 100 µl 1/10 serially diluted supernatants for 5 days at 37 °C. Then, $TCID_{50}$ was determined by assessing CPEs in each well by light microscopy, and the 50% endpoint was calculated according to the method of Reed and Muench[59].

**IAV-NLuc production and infection.** A/Victoria/3/75 virus carrying a NLuc reporter gene generation and production have been described[53]. Viruses were amplified on MDCK cells cultured in serum-free DMEM containing 0.5 µg $ml^{-1}$ L-1-p-Tosylamino-2-phenylethyl chloromethyl ketone (TPCK)-treated trypsin (Sigma-Aldrich). Stocks were titrated by plaque assays on MDCK cells (typical titers were $10^7$ plaque-forming units per milliliter). IAV-NLuc challenges were performed in 96-well plates in serum-free DMEM for 1 h, and the medium was subsequently replaced with DMEM containing 10% FBS. Cells were lysed 10 h later, and NLuc activity was measured with the Nano-Glo assay system (Promega) and an Infinite 200 PRO plate reader (Tecan).

**SARS-CoV-2 internalization assay.** Calu-3 cells were incubated with SARS-CoV-2 at an m.o.i. of 5 for 2 h at 37 °C, washed twice with PBS and then treated with Subtilisin A (400 µg $ml^{-1}$) in Subtilisin A buffer (10 mM Tris/HCl (pH 8.0), 150 mM NaCl and 5 mM $CaCl_2$) to get rid of the cell surface-bound viruses before washes, lysis, RNA extraction (RNeasy kit, Qiagen) and RdRp RT-qPCR to measure the relative amounts of internalized viruses.

**Spike pseudotype production.** 293 T cells were seeded in plates precoated with poly-lysine (Sigma-Aldrich) and transfected with 5 µg of an expression plasmid coding either VSV-G (pMD.G) or SARS-CoV-2 spike del19 (pcDNA3.1_spike_del19) using Lipofectamine 2000 (Thermo Fisher Scientific). The culture medium was replaced after 6 h. Cells were infected 24 h after transfection with VSVΔG-GFP-Firefly Luciferase (a gift from G. Zimmer[34]) at a m.o.i. of 5 for 1 h at 37 °C and washed three times with PBS. The medium was replaced with 5% FCS-supplemented DMEM containing 1 µg $ml^{-1}$ of an anti-VSV-G antibody (CliniSciences, clone 8G5F11) to neutralize residual viral input[60]. Supernatants were harvested 24 h later, spun at 1,000 *g* for 10 min and stored at −80 °C.

**RNA quantification.** RNA was extracted using the RNeasy kit (Qiagen) using on-column DNase treatment, according to the manufacturer's instructions, reverse-transcribed and subjected to qPCR. All sequences and references of primers and probes are described in Supplementary Table 2 (ref. [61,62]). Triplicate reactions were run using a ViiA7 Real Time PCR system (Thermo Fisher Scientific). pRdRp[22] and pNL63 (which contains a fragment amplified from NL63-infected cell RNAs using primers NL63_F2 and NL63_R2 and cloned into pPCR-Blunt II-TOPO) were diluted in 20 ng $ml^{-1}$ salmon sperm DNA to generate a standard curve to calculate relative cDNA copy numbers and confirm the assay linearity (detection limit: 10 molecules per reaction).

**ACE2 staining using spike RBD-mFc recombinant protein and flow cytometry analysis.** The SARS-CoV-2 spike RBD sequence was obtained from RNA extracted from a patient sample collected in Montpellier University hospital and a gift from V. Foulongne[63] (GenBank accession number MT787505.1). The predicted N-terminal signal peptide of spike (amino acids 1–14) was fused to the RBD sequence (amino acids 319–541), C-terminally tagged with a mouse IgG1 Fc fragment (mFc) and cloned into pCSI vector[64]. The pCSI-spikeRBD expression vector was transfected in HEK293T cells using the PEIpro transfection reagent. Cells were washed 6 h after transfection and grown for an additional 72–96 h in serum-free Optipro medium (Invitrogen) supplemented with glutamine and non-essential amino acids. Supernatant was harvested, filtered and concentrated 100-fold on 10 kDa-cutoff Amicon Ultra-15 concentrators. Samples were aliquoted and stored at −20 °C until further use. The spike RBD-mFc validation is presented in Supplementary Fig. 2.

For ACE2 labeling, cells were harvested using PBS-5 mM EDTA, incubated 20 min at 37 °C in FACS buffer (PBS1X-2% BSA) containing a 1:20 dilution of spike RBD-mFc, followed by secondary anti-mouse Alexa Fluor 488 incubation (Thermo Fisher Scientific; 1:1,000 dilution) and several washes in FACS buffer. Flow cytometry was performed using NovoCyte (ACEA Biosciences) and analyzed using FlowJo software.

**Immunoblot analysis.** Cells were lysed in lysis buffer (10 mM Tris 1 M (pH 7.6), NaCl 150 mM, Triton X100 1%, EDTA 1 mM and deoxycholate 0.1%) supplemented with sample buffer (50 mM Tris-HCl (pH 6.8), 2% SDS, 5% glycerol, 100 mM DTT and 0.02% bromophenol blue), resolved by SDS-PAGE and analyzed by immunoblotting using primary antibodies against ACE2 (ProteinTech 21115-1-P; diluted 1:1,000), AP1G1 (Bethyl Laboratories, A304-771A; 1:1,000), AP1B1 (Proteintech, 16932-1-AP; 1:500), AAGAB (Bethyl Laboratories, A305-593A; 1:1,000), or Actin (Sigma-Aldrich, A1978; 1:5,000), followed by horseradish peroxidase-conjugated anti-rabbit or anti-mouse immunoglobulin antibodies (Thermo Fisher Scientific; 1:2,500), or using an anti-GAPDH antibody conjugated to horseradish peroxidase (Sigma-Aldrich, G9295; 1:5,000) and chemiluminescence Clarity or Clarity Max substrate (Bio-Rad). A Bio-Rad ChemiDoc imager was used. Unprocessed immunoblot images are available as Source Data.

**TPCK-treated trypsin priming of S.** Cells were treated or not with camostat mesylate (Sigma-Aldrich) at a concentration of 100 µM at 37 °C for 1 h, placed on ice and incubated with wild-type SARS-CoV-2 (m.o.i. 1.25), SARS-CoV-2 mNG reporter (m.o.i. 0.01) or VSV pseudoparticles (m.o.i. 0.1) for 30 min on ice. Cells were extensively washed with PBS1X to remove the unbound viruses (and the 'inputs' were collected by lysis in RLT buffer) before TPCK-treated trypsin (Sigma-Aldrich) treatment, as follows.

For single-round infections (i.e., with wild-type SARS-CoV-2 and VSV pseudoparticles), exogenous priming of spike was achieved by incubation with TPCK-treated trypsin at 100 µg ml$^{-1}$ in serum-free DMEM at 37 °C for 10 min. Cells were washed with 5% FCS-DMEM to neutralize the trypsin and cultured in 5% FCS-DMEM in the presence of 100 µM camostat or not. For wild-type SARS-CoV-2 infections, cells were lysed in RLT buffer at 7 h after infection, RNA extracted (RNeasy kit, Qiagen) and SARS-CoV-2 RdRp RNAs measured by RT-qPCR. For VSV pseudoparticle infections, cells were lysed 30 h after infection in Passive Lysis buffer, and Firefly luciferase activity was measured with the luciferase assay system (Promega) and the Infinite 200 PRO plate reader (Tecan).

For multiple-round SARS-CoV-2 mNG experiments, exogenous priming of spike was achieved with the continuous presence of TPCK-treated trypsin (at 5 µg ml$^{-1}$) in serum-free medium, throughout the experiment. Cells were trypsinized 24 h or 48 h after infection (for + camostat and CTRL conditions, respectively), and the percentage of cells expressing mNG was scored by flow cytometry (NovoCyte, ACEA Biosciences) after fixation in PBS1X-2% PFA.

**Analysis of scRNA-seq data.** For published scRNA-seq data analysis, Seurat objects were downloaded from figshare (https://doi.org/10.6084/m9.figshare.12436517.v2 (ref. [33])). Cell identities and CRISPR hits were selected and plotted using the DotPlot function in Seurat[33].

**Statistical analysis and reproducibility.** Statistical analyses were performed using Prism software or Excel (*$P<0.05$, **$P<0.01$, ***$P<0.001$, ****$P<0.0001$). Experiments were performed in biological replicates, and the exact number of repeats is provided in the figure legends and/or Supplementary Data 17.

**Reporting summary.** Further information on research design is available in the Nature Research Reporting Summary linked to this article.

## Data availability

The datasets generated during and/or analyzed during the current study have been deposited to the Gene Expression Omnibus (primary screen data: GSE175666; secondary screen data: GSE193834). Additional data are available from the corresponding authors on reasonable request.
Requests for material should be addressed to C.G. or J.G.D. or Addgene (for the plasmids with an Addgene number). Source data are provided with this paper.

## Code availability

All code used in this study can be found on GitHub (https://github.com/PriyankaRoy5/SARS-CoV-2-meta-analysis) and Zenodo[65] (https://doi.org/10.5281/zenodo.6499838).

## References


49. Konermann, S. et al. Genome-scale transcriptional activation by an engineered CRISPR-Cas9 complex. *Nature* **517**, 583–588 (2015).
50. DeWeirdt, P. C. et al. Optimization of AsCas12a for combinatorial genetic screens in human cells. *Nat. Biotechnol.* **39**, 94–104 (2021).
51. Sanjana, N. E., Shalem, O. & Zhang, F. Improved vectors and genome-wide libraries for CRISPR screening. *Nat. Methods* **11**, 783–784 (2014).
52. Shalem, O. et al. Genome-scale CRISPR-Cas9 knockout screening in human cells. *Science* **343**, 84–87 (2014).
53. Doyle, T. et al. The interferon-inducible isoform of NCOA7 inhibits endosome-mediated viral entry. *Nat Microbiol* **3**, 1369–1376 (2018).
54. Nakabayashi, H., Taketa, K., Miyano, K., Yamane, T. & Sato, J. Growth of human hepatoma cells lines with differentiated functions in chemically defined medium. *Cancer Res.* **42**, 3858–3863 (1982).
55. Zhong, J. et al. Robust hepatitis C virus infection in vitro. *Proc. Natl Acad. Sci. USA* **102**, 9294–9299 (2005).
56. Xie, X. et al. A nanoluciferase SARS-CoV-2 for rapid neutralization testing and screening of anti-infective drugs for COVID-19. *Nat. Commun.* **11**, 5214 (2020).
57. van den Worm, S. H. E. et al. Reverse genetics of SARS-related coronavirus using vaccinia virus-based recombination. *PLoS One* **7**, e32857 (2012).
58. Almazán, F. et al. Engineering a replication-competent, propagation-defective middle east respiratory syndrome coronavirus as a vaccine candidate. *mBio* **4**, e00650 (2013).
59. Reed, L. J. & Muench, H. A simple method of estimating fifty per cent endpoints12. *American Journal of Epidemiology* **27**, 493–497 (1938).
60. Condor Capcha, J. M. et al. Generation of SARS-CoV-2 spike pseudotyped virus for viral entry and neutralization assays: a 1-week protocol. *Front. Cardiovasc. Med.* **7**, 618651 (2020).
61. Corman, V. M. et al. Detection of 2019 novel coronavirus (2019-nCoV) by real-time RT-PCR. *Eur. Surveill.* **25**, 2000880 (2020).
62. Carbajo-Lozoya, J. et al. Replication of human coronaviruses SARS-CoV, HCoV-NL63 and HCoV-229E is inhibited by the drug FK506. *Virus Res.* **165**, 112–117 (2012).
63. Veyrenche, N. et al. Diagnosis value of SARS-CoV-2 antigen/antibody combined testing using rapid diagnostic tests at hospital admission. *J. Med. Virol.* **93**, 3069–3076 (2021).
64. Giovannini, D., Touhami, J., Charnet, P., Sitbon, M. & Battini, J.-L. Inorganic phosphate export by the retrovirus receptor XPR1 in metazoans. *Cell Rep.* **3**, 1866–1873 (2013).
65. Roy, P. *PriyankaRoy5/SARS-CoV-2-meta-analysis: bidirectional genome-wide CRISPR screens reveal host factors regulating SARS-CoV-2, MERS-CoV and seasonal HCoVs* (Zenodo, 2022). https://doi.org/10.5281/zenodo.6499838


## Acknowledgements

We thank S. Van der Werf from the French National Reference Centre for Respiratory Viruses (Pasteur Institute, Paris, France) for providing us with SARS-CoV-2 BetaCoV/France/IDF0372/2020 (isolated by X. Lescure and Y. Yazdanpanah, Bichat Hospital); the World Reference Center for Emerging Viruses and Arboviruses and UTMB investigator P. Yong Shi for the mNeonGreen and NLuc reporter SARS-CoV-2; V. Thiel for Renilla reporter HCoV-229E; BEI Resources, NIAID, NIH for providing us with HCoV-NL63. We thank R. Gaudin, L. Chauveau, L. Espert, V. Hebmann, C. Chable-Bessia, B. Beaumelle, Nathalie Arhel, M. Sitbon, V. Foulongne, C.-Y. Lin, G. Zimmer and R. De Francesco for the generous provision of reagents, and we thank M. Moriel-Carretero, P.-Y. Lozach and L. Picas for helpful discussions. We are grateful to C. Chable-Bessia and all CEMIPAI BSL-3 facility members for setting up excellent working conditions for SARS-CoV-2 handling. This work was supported by the French National Research Agency (ANR) under the ANR-RA COVID program (grant ANR-20-COV6-0001, CRISPR-TARGET-CoV, to C.G.); a European Research Council (ERC) Starting Grant under the European Union's Horizon 2020 research and innovation program (grant agreement 759226, ANTIViR, to C.G.); the Institut National de la Santé et de la Recherche Médicale (INSERM) (C.G. and M.W.); the Fondation Centre National de la Recherche Scientifique (CNRS) (C.G. and O.M.); institutional funds from CNRS, Institut des Sciences Biologiques du CNRS and Montpellier University (C.G. and O.M.); 3-year PhD studentships from the Ministry of Higher Education and Research (A.R., B.B. and J.M.); 4th-year PhD funding from the Fondation pour la Recherche Médicale (B.B. and J.M.); NIAID grant R21AI157835 (J.G.D.); and the COVID program from CNRS (L.D.). We acknowledge the imaging facility MRI, a member of the national infrastructure France-BioImaging supported by the French National Research Agency (ANR-10-INBS-04) and the CEMIPAI BSL-3 facility.

## Author contributions

A.R., P.R., J.G.D. and C.G. conceived the study; A.R. and C.G. designed the experiments; A.R. and C.G. performed the CRISPR screens; P.R., M.H., P.D.W. and J.G.D. performed the computational analysis; A.R., B.B., A.L.C.V., L.D., O.M. and C.G. performed the BSL-2 and BSL-3 experiments; M.A.A., Y.R., M.T., and Y.L. provided technical help; D.G. provided spike RBD-mFc for ACE2 staining and J.T. validated this tool; S.U. and K.E.K did the mass spectrometry analyses; F.G.d.G, J.M. and M.W. participated in data interpretation. J.G.D. and C.G. provided overall supervision along with S.B. and J.D.; A.R., P.R., J.G.D. and C.G. wrote the manuscript with input from all authors.

## Competing interests

J.G.D. consults for Agios, Microsoft Research, Phenomic AI, BioNTech and Pfizer; J.G.D consults for and has equity in Tango Therapeutics. J.G.D.'s interests were reviewed and are managed by the Broad Institute in accordance with its conflict-of-interest policies. The other authors declare no competing interests.

## Additional information

**Extended data** is available for this paper at https://doi.org/10.1038/s41588-022-01110-2.

**Supplementary information** The online version contains supplementary material available at https://doi.org/10.1038/s41588-022-01110-2.

**Correspondence and requests for materials** should be addressed to John G. Doench or Caroline Goujon.

**Peer review information** *Nature Genetics* thanks Zharko Daniloski and the other, anonymous, reviewer(s) for their contribution to the peer review of this work. Peer reviewer reports are available.

**Reprints and permissions information** is available at www.nature.com/reprints.

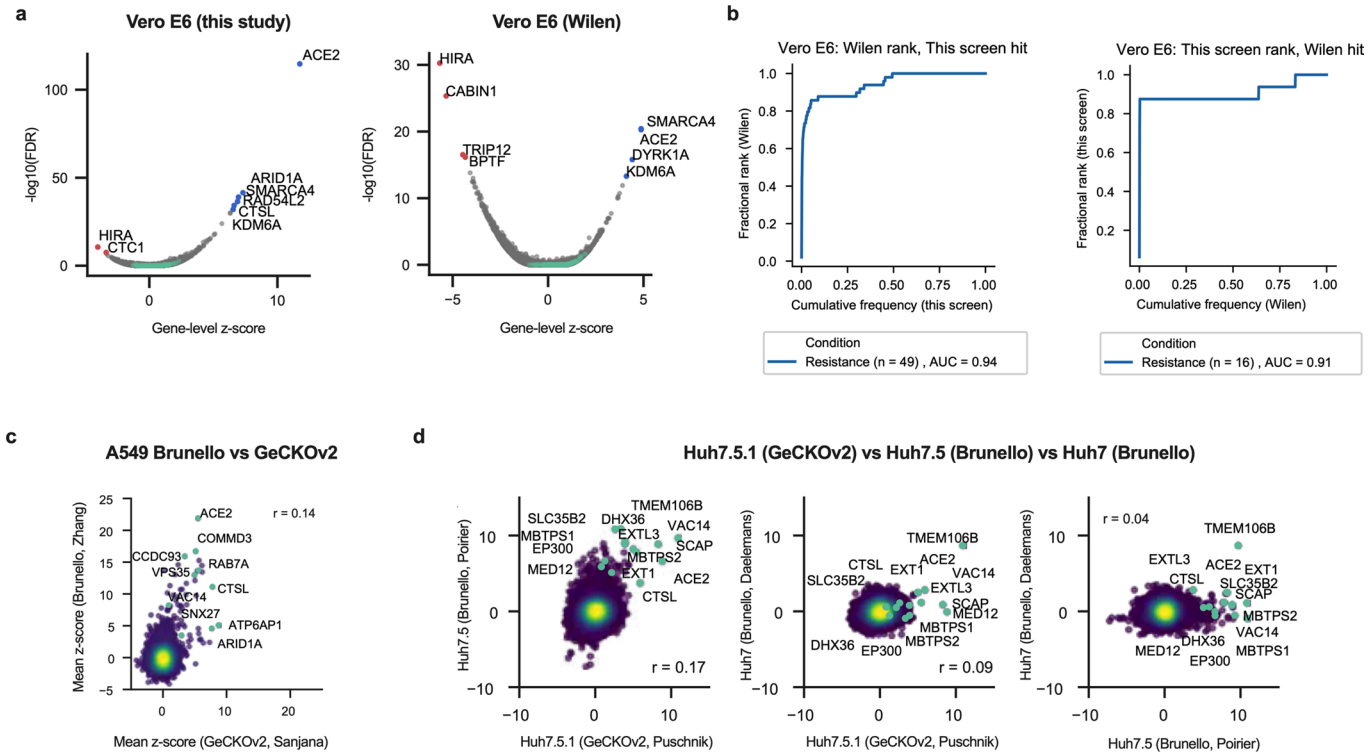


**Extended Data Fig. 1 | Meta-analysis of genome-wide screens. a**. Volcano plot showing the top genes conferring resistance (right, blue) and sensitivity (left, red) to SARS-CoV-2 when knocked out in Vero E6 cells for this screen (left panel) and the screen conducted by Wei et al. 2021 (Wilen[20]; right panel). Controls are indicated in green. The gene-level z-score and -log10(FDR) were calculated after averaging across conditions (of note, the FDR value for ACE2 is effectively zero but has been assigned a -log(FDR) value for plotting purposes). ($n = 20{,}928$ for each plot). **b**. Cumulative distribution plots analyzing overlap of top hits between this screen and the Wilen screen. Left panel: Putative hit genes from the Wilen screen are ranked by mean z-score, and classified as validated hits based on mean z-score in the secondary screen, using a threshold of greater than 3. Right panel: Putative hit genes from this screen are ranked by mean z-score, and classified as validated hits based on mean z-score in the Wilen screen, using a threshold of greater than 3. **c**. Comparison between genome-wide screens conducted in A549 cells overexpressing ACE2 by Daniloski et al. (Sanjana[17]) and Zhu et al. (Zhang[21]) using the GeCKOv2 and Brunello libraries, respectively. Pearson's correlation coefficient r is indicated. ($n = 18{,}484$). **d**. Pair-wise comparison between genome-wide screens conducted in Huh7.5.1-ACE2-TMPRSS2, Huh7.5, and Huh7 cells by Wang et al. (Puschnik[19]), Schneider et al. (Poirier[18]), and Baggen et al. (Daelemans[16]), respectively, using the GeCKOv2 and Brunello libraries as indicated. Annotated genes include top 3 resistance hits from each screen as well as genes that scored in multiple cell lines based on the criteria used to construct the Venn diagram in Fig. 1d. Pearson's correlation coefficient r is indicated. ($n = 18{,}470$ for each plot).

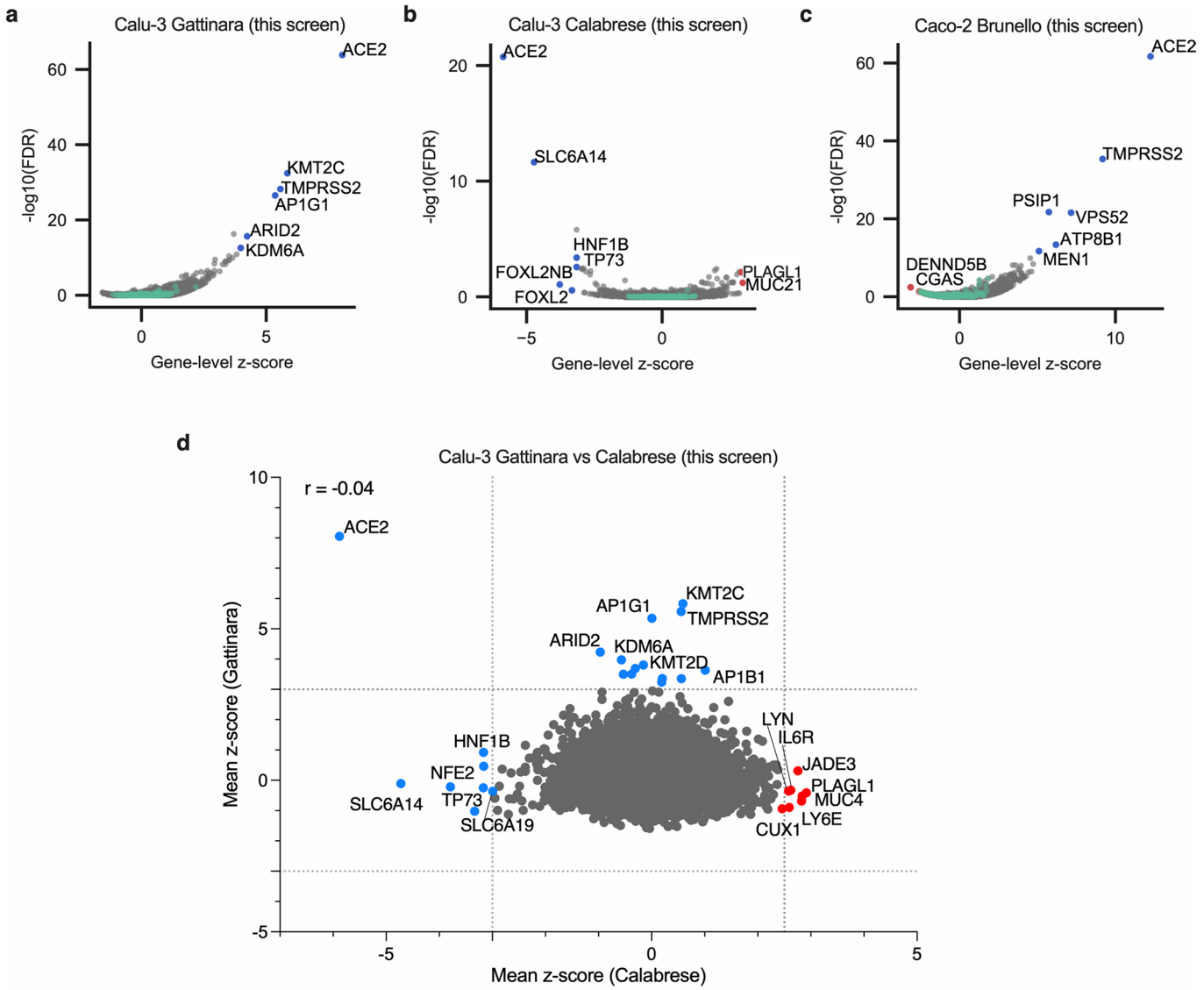


**Extended Data Fig. 2 | Genome-wide CRISPR KO and CRISPRa screens in Calu-3 and Caco-2 cells. a**. Volcano plot showing the top genes conferring resistance (right, blue) to SARS-CoV-2 when knocked out in Calu-3 cells. Controls are indicated in green. This screen did not have any sensitization hits. The gene-level z-score and –log10(FDR) were calculated after averaging across replicates. ($n = 20,513$). **b**. Volcano plot showing the top genes conferring resistance (right, red) and sensitivity (left, blue) to SARS-CoV-2 when overexpressed in Calu-3 cells. Controls are indicated in green. The gene-level z-score and –log10(FDR) were calculated after averaging across replicates. ($n = 20,494$). **c**. Volcano plot showing the top genes conferring resistance (right, blue) and sensitivity (left, red) to SARS-CoV-2 when knocked out in Caco-2 cells. Controls are indicated in green. The gene-level z-score and –log10(FDR) were calculated after averaging across replicates. ($n = 18,804$). **d**. Comparison between gene hits in Calu-3 KO and activation screens. Dotted lines indicated mean z-scores of -3 and 2.5 or 3 for each screen. Proviral and antiviral genes are indicated in blue and red, respectively. Pearson's correlation coefficient r is indicated. ($n = 18,173$).

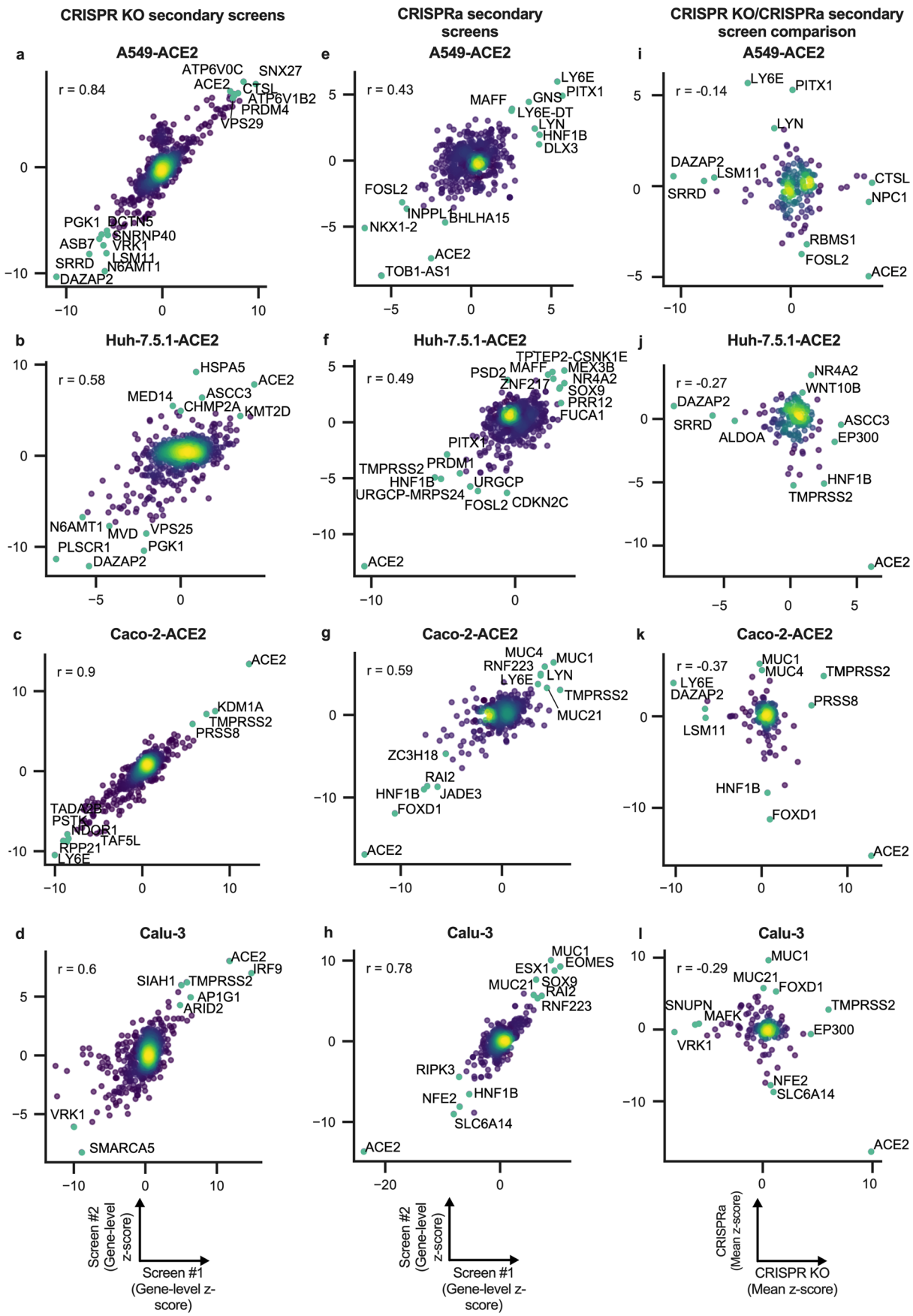


**Extended Data Fig. 3 | See next page for caption.**

**Extended Data Fig. 3 | Secondary screens in A549-ACE2, Huh7.5.1-ACE2, Caco-2-ACE2 and Calu-3 cells. a-d**. Scatter plots showing gene-level z-scores for each secondary activation screen with top resistance and sensitization hits annotated (A549-ACE2, Huh7.5.1-ACE2, Caco-2-ACE2 and Calu-3, respectively). Pearson's correlation coefficient, r, is labeled (n = 677, each). **e-h**. Scatter plots showing gene-level z-scores for each secondary activation screen with top resistance and sensitization hits annotated (A549-ACE2, Huh7.5.1-ACE2, Caco-2-ACE2 and Calu-3, respectively). Pearson's correlation coefficient, r, is labeled (n = 820, each). **i-l**. Scatter plots showing mean z-scores comparing each secondary activation screen to each secondary KO screen for each cell line with top resistance and sensitization hits annotated (A549-ACE2, Huh7.5.1-ACE2, Caco-2-ACE2 and Calu-3). Pearson's correlation coefficient, r, is labeled (n = 179, each).

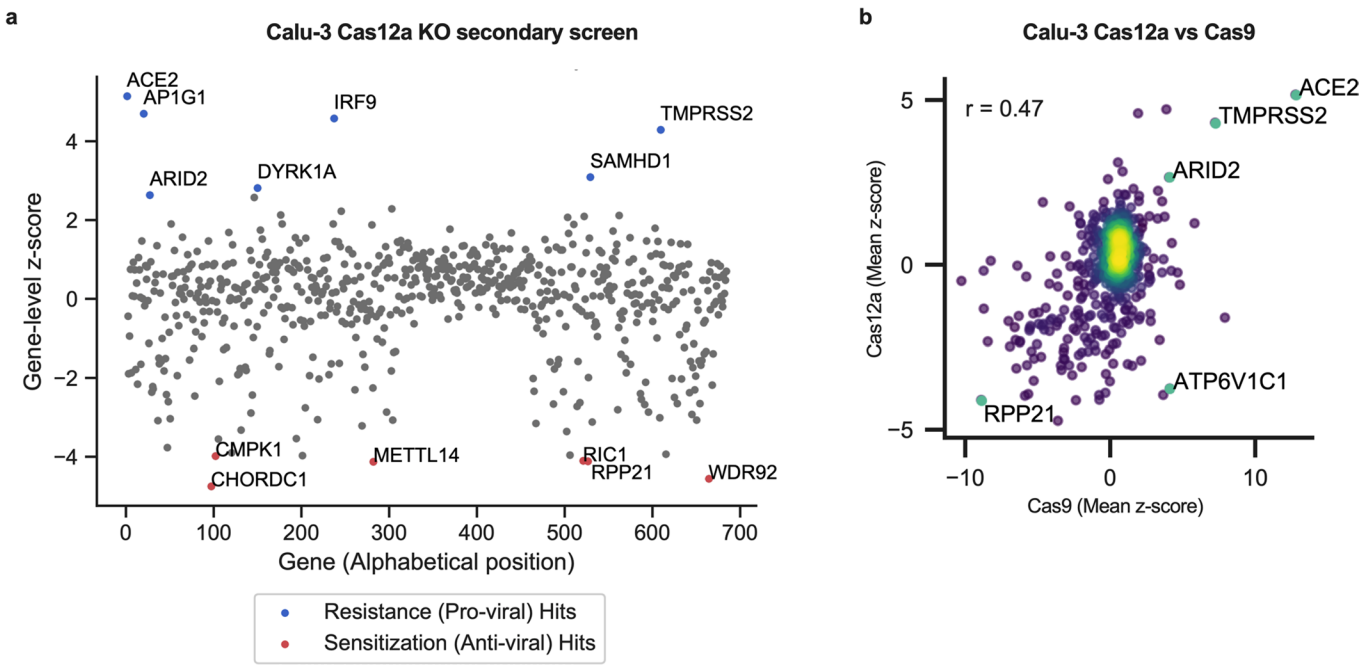


**Extended Data Fig. 4 | Secondary KO screen in Calu-3-Cas12a cells and comparison with Cas9-based screens. a**. Scatter plot showing the gene-level z-scores of genes when knocked out using Cas12a in Calu-3 cells. The top genes conferring resistance to SARS-CoV-2 are annotated and shown in blue. The top genes conferring sensitivity to SARS-CoV-2 are annotated and shown in red. (n = 684). Only one replicate is shown as the second replicate had low sequencing quality. **b**. Scatter plots showing mean z-scores comparing each Cas9 to Cas12a secondary KO screens for Calu-3 cells with top resistance and sensitization hits annotated. Pearson correlation, r, labeled (n = 600 each).

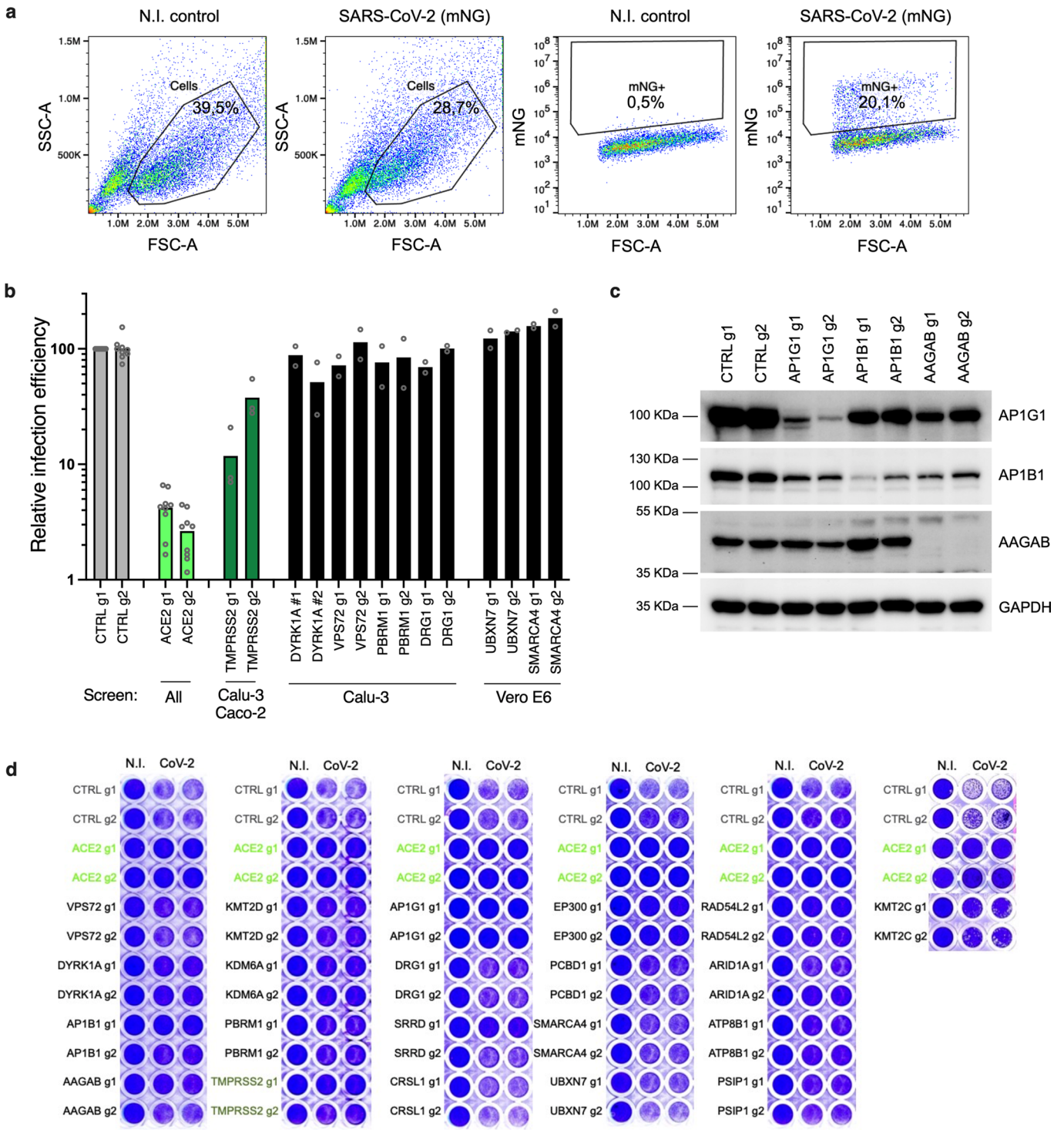


**Extended Data Fig. 5 | Proviral gene candidate validation in Calu-3 cells. a. Gating strategy for flow cytometry analysis**. Pseudocolored dot-plots of sorted Calu-3 cells, showing gates used for the analysis in Fig. 3a (and all figures using flow cytometry analysis). **b. Impact of additional candidate gene KO** (panel complementary to Fig. 4a). Calu-3-Cas9 cells were stably transduced to express 2 different sgRNAs (g1, g2) per indicated gene and selected. Cells were infected with SARS-CoV-2 bearing the mNeonGreen (mNG) reporter and the infection efficiency was scored 48 h later by flow cytometry. The cell line/screen in which the candidates were identified is indicated below the graph; data from 2 independent experiments are shown. **c**. ***AP1G1***, ***AP1B1,*** **and *AAGAB* depletion efficiency in Calu-3 KO cell populations**. A representative immunoblot is shown out of 3 independent experiments; GAPDH serves as a loading control. **d. SARS-CoV-2-induced cytopathic effects in KO cell lines**. Calu-3-Cas9 cells were stably transduced to express 2 different sgRNAs (g1, g2) per indicated gene and selected. Cells were infected by SARS-CoV-2 at MOI 0.005 and ~5 days later stained with crystal violet. Representative images out of 2 independent experiments are shown.

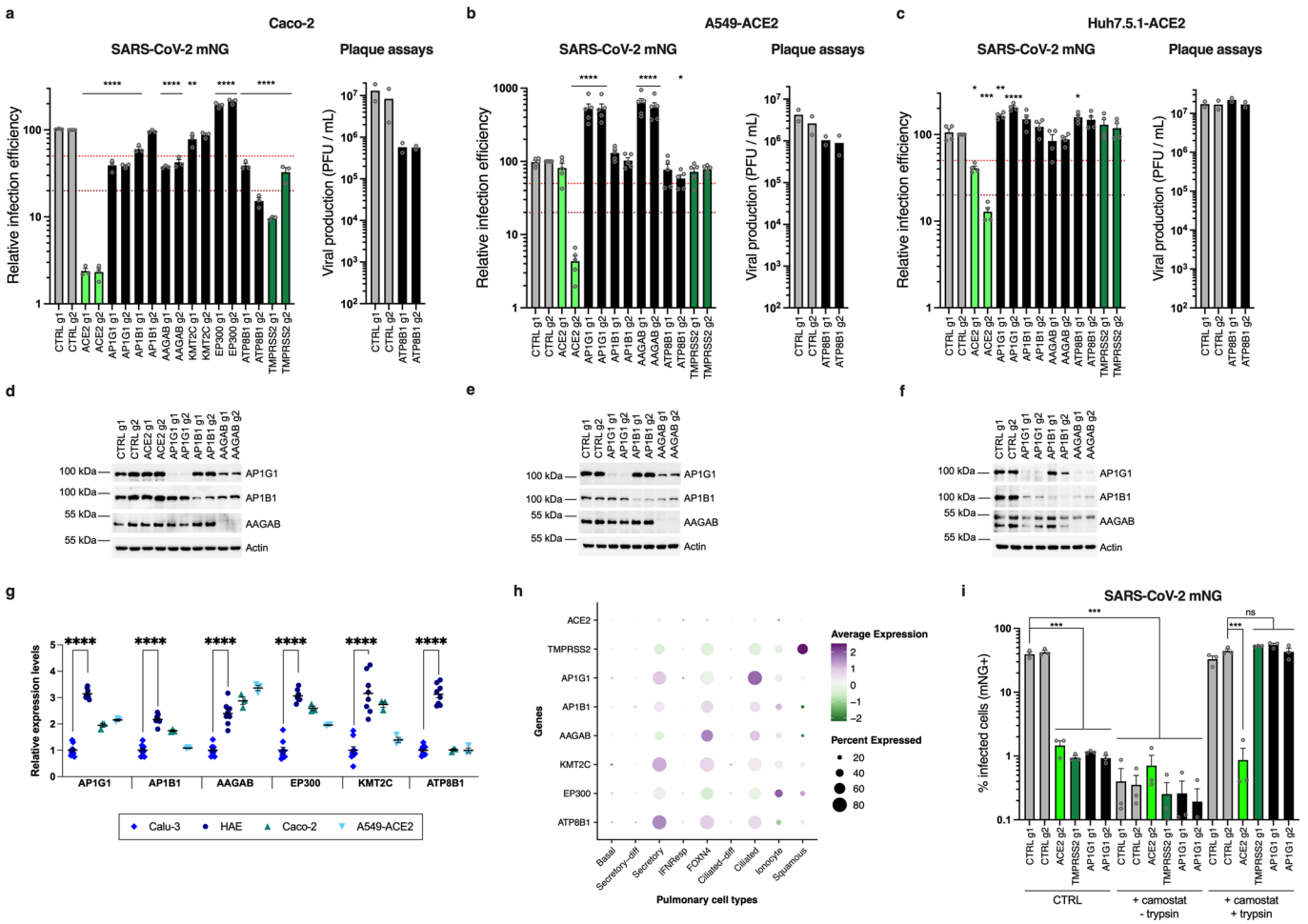


**Extended Data Fig. 6 | Proviral gene candidate validation in other cell lines. a**. Caco-2-Cas9 cells expressing 2 sgRNAs (g1, g2) per indicated gene were infected with SARS-CoV-2 mNG reporter. Infection efficiency scored 48 h later by flow cytometry (left panel). In parallel, supernatants were collected and virus production determined by plaque assays (right panel). Mean and s.e.m. of 3 (left) and mean of 2 (right) independent experiments are shown, respectively. **b**. Similar to **a**, with A549-ACE2 cells. Mean and s.e.m. of 5 (left) and mean of 2 (right) independent experiments. **c**. Similar to **a**, with Huh7.5.1-ACE2 cells. Mean and s.e.m. of 4 independent experiments (left) or a representative experiment (with technical duplicates) is shown (right). **a-c**. One-way ANOVA with Dunnett's test (* $p < 0.05$, ** $p < 0.01$, *** $p < 0.001$, **** $p < 0.0001$). Of note, ACE2 g1 targets an intron-exon junction on *ACE2* endogenous sequence and cannot target *ACE2* ectopic CDS in ACE2-transduced cells. **d-f**. Expression levels of AP1G1, AP1B1 and AAGAB in Caco-2 (**d**), A549-ACE2 (**e**) and Huh7.5.1-ACE2 (**f**) KO cells were analyzed by immunoblot, Actin served as a loading control. A representative immunoblot is shown (from 3 independent experiments). **g**. RNA samples from 9 (HAE from different donors[22]), 8 (Calu-3), or 3 (Caco-2, A549-ACE2) independent experiments were analyzed by RT-qPCR. Statistical significance was determined by unadjusted, two-sided Mann-Whitney test (**** $p < 0.0001$). **h**. Candidate gene expression levels in cell types from the respiratory epithelium (from Chua et al.[33]). Expression levels in COVID-19 versus healthy patients are color coded; the percentage of cells expressing the respective gene is size coded, as indicated. **i**. Cells were pretreated for 1 h with camostat mesylate or not, incubated with SARS-CoV-2 mNG on ice and washed. The media was replaced with serum-free media containing trypsin in order to prime Spike, or no trypsin. Infection efficiency was analyzed by flow cytometry after 24 h (for the + camostat conditions) or after 48 h (for CTRL). Statistical significance was determined by two-sided t-tests with no adjustment for multiple comparisons (* $p < 0.05$, ** $p < 0.01$, *** $p < 0.001$, **** $p < 0.0001$). The exact n and p-values (**a, b, c, g, i**) are indicated in Supplementary Data 17.

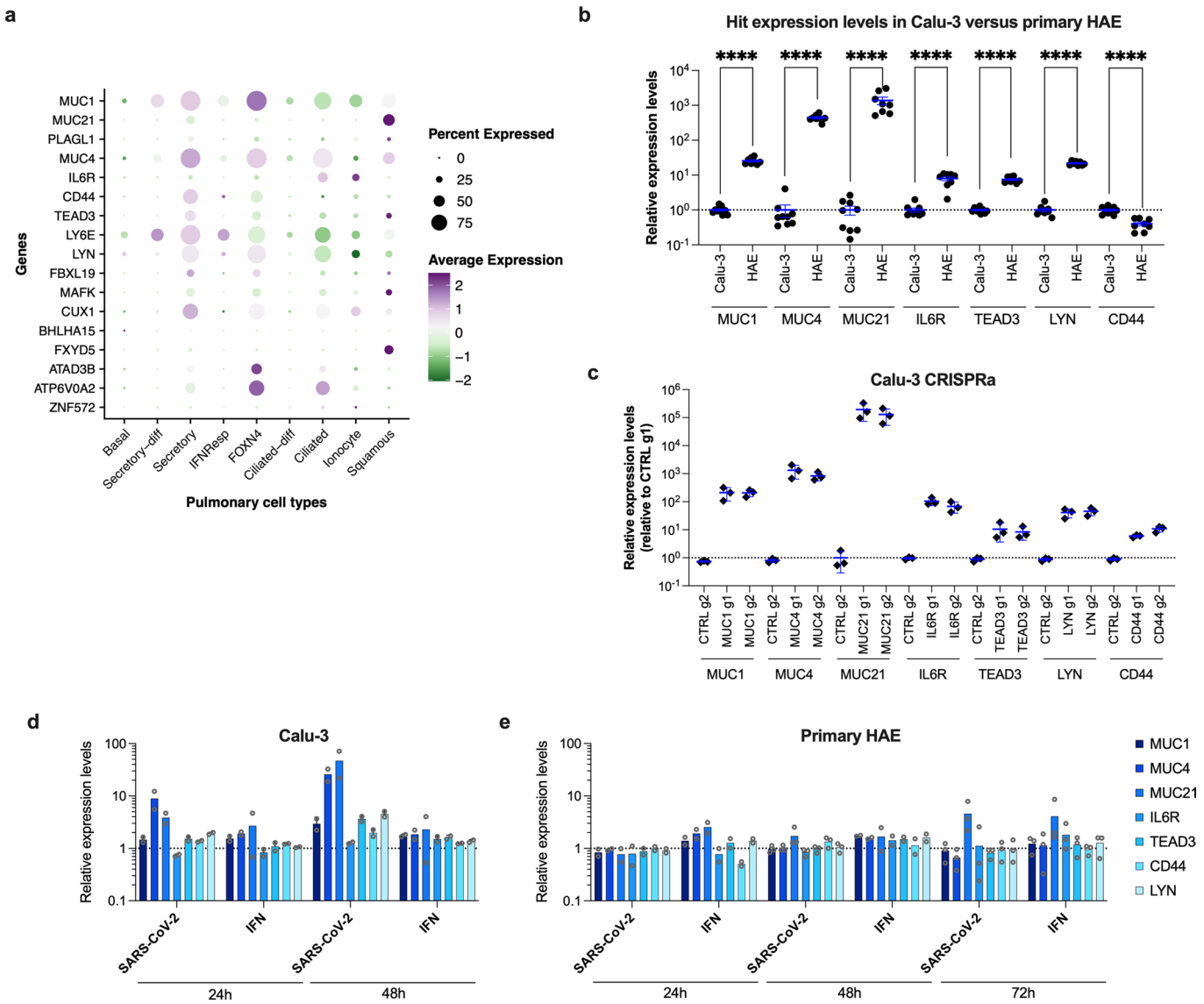


**Extended Data Fig. 7 | Antiviral gene expression levels. a. Dot plot depicting the expression levels of the best validated antiviral genes in the different cell types from the respiratory epithelium**, from Chua et al. data set[33]. Expression levels in COVID-19 versus healthy patients are color coded; the percentage of cells expressing the respective gene is size coded, as indicated. **b. Relative expression levels of a selection of antiviral factors in primary human airway epithelial cells (HAE) compared to Calu-3 cells**. RNA samples from 9 and 8 independent experiments for HAE and Calu-3, respectively (described in[22], as in Extended Data Fig. 6g), were analyzed by RT-qPCR using the indicated taqmans (samples were normalized with ActinB and GAPDH). Statistical significance was determined by unadjusted, two-sided Mann-Whitney test (**** $p < 0.0001$). The exact n and p-values (**b**) are indicated in Supplementary Data 17**. c. Relative expression levels of the antiviral hits in CRISPRa Calu-3 cells**. RNA samples from 3 independent experiments (corresponding to Fig. 6) were analyzed by RT-qPCR using the indicated taqmans (samples were normalized with ActinB and GAPDH); relative expression levels compared to CTRL g1 populations are shown. **d-e. Impact of SARS-CoV-2 infection and interferon treatment on antiviral factor expression in Calu-3 cells (d) and primary HAE (e)**, as indicated, in samples from ≥ 2 independent experiments from our previous study[22].

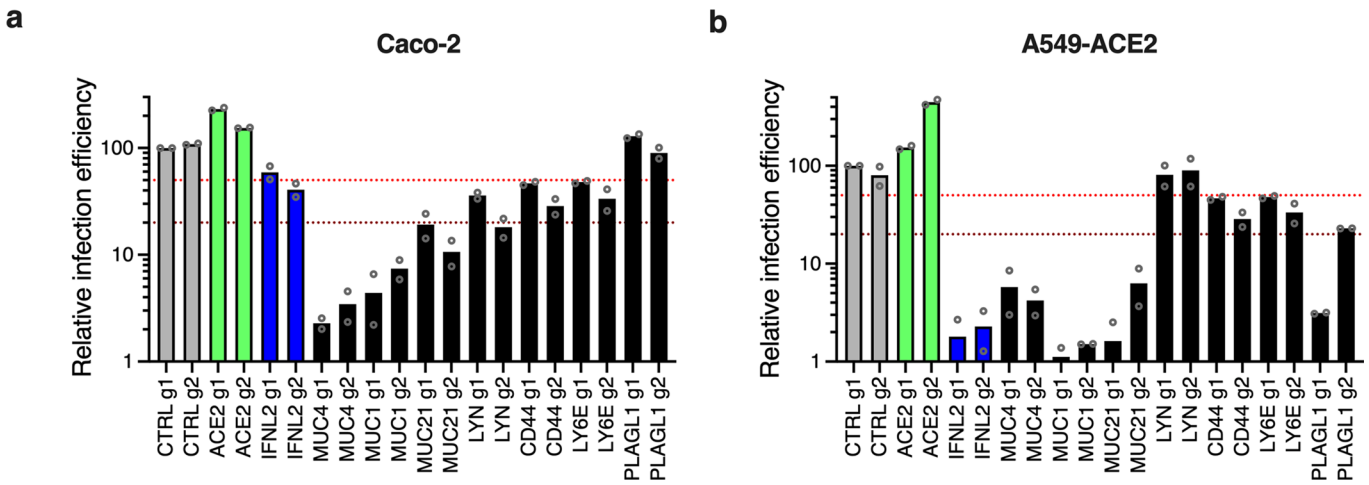


**Extended Data Fig. 8 | Impact of the identified antiviral genes on SARS-CoV-2 in Caco-2 and A549-ACE2 cells.** Caco-2-dCas9-VP64 (**a**) and A549-ACE2-dCas9-VP64 (**b**) cells were stably transduced to express 2 different sgRNAs (g1, g2) per indicated gene promoter, or negative controls (CTRL) and selected prior to SARS-CoV-2 mNG infection. The percentage of infected cells was scored 48 h later by flow cytometry. The mean of relative infection efficiencies are shown for 2 independent experiments. The red and dark red dashed lines represent 50% and 80% inhibition, respectively.

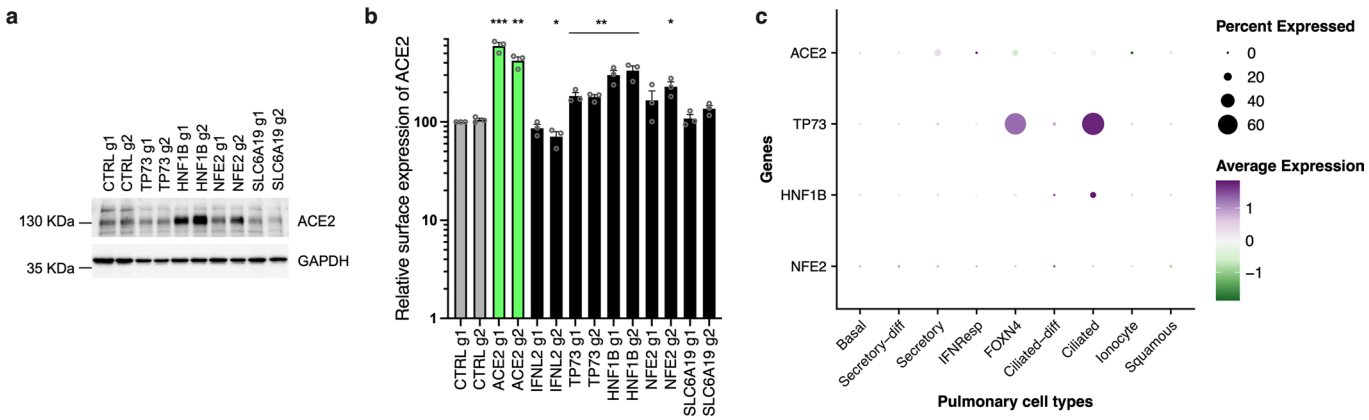


**Extended Data Fig. 9 | Characterization of proviral genes identified by CRISPRa. a-b. ACE2 expression in CRISPRa cell lines. Calu-3**-Cas9 cells were stably transduced to express 2 different sgRNAs (g1, g2) per indicated gene and selected (parallel samples from Fig. 8). **a**. The cells were lysed and expression levels of ACE2 were analyzed, Actin served as a loading control A representative immunoblot (out of 2 independent experiments) is shown. **b**. ACE2 surface staining using Spike-RBD-mFc. Mean and SEM of 3 independent experiments. Statistical significance was determined by a two-sided t-test (* $p < 0.05$, ** $p < 0.01$, *** $p < 0.001$, **** $p < 0.0001$). **c. Dot plot depicting the expression levels of the best validated proviral genes in the different cell types from the respiratory epithelium**, from Chua et al. data set[33]. Expression levels in COVID-19 versus healthy patients are color coded; the percentage of cells expressing the respective gene is size coded, as indicated.

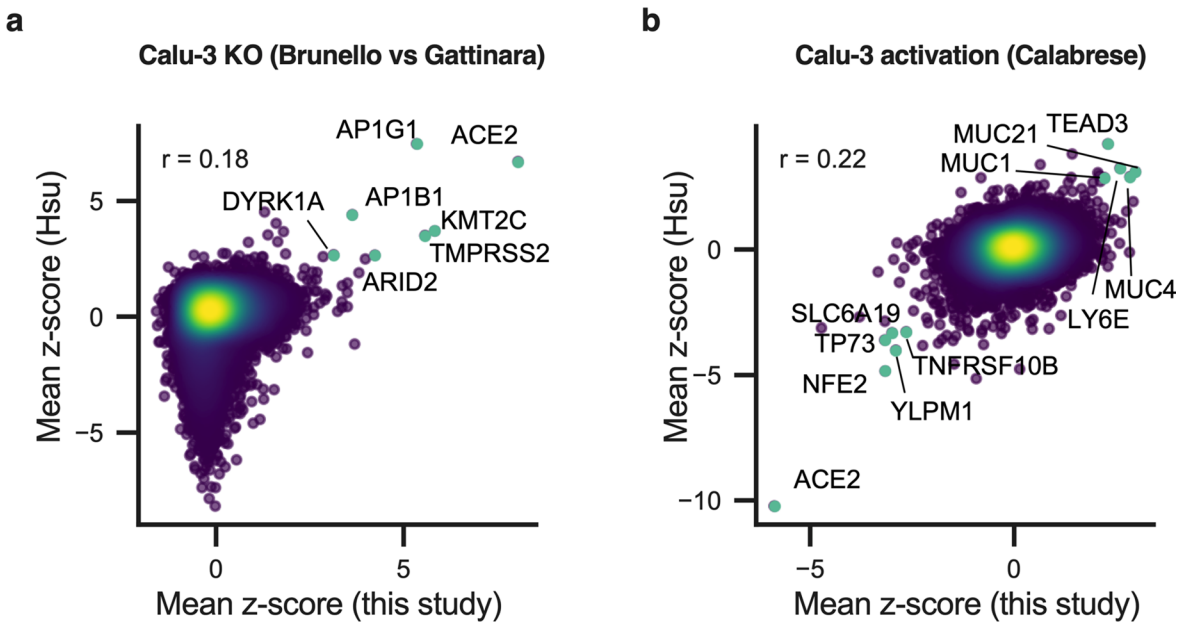


**Extended Data Fig. 10 | Bidirectional screen data comparison between this study and Hsu et al's. a**. Comparison between this Calu-3 KO screen to the Calu-3 KO screen conducted by Hsu and colleagues[45]. Genes that scored among the top 20 resistance hits in both screens are annotated and shown in green. Pearson's correlation coefficient r is indicated. **b**. Comparison between this Calu-3 activation screen to the Calu-3 activation screen conducted by Hsu and colleagues[45]. Genes that scored among the top 20 resistance hits and sensitization hits in both screens are annotated and shown in green. Pearson's correlation coefficient r is indicated.

nature research

Corresponding author(s): C. Goujon / J. Doench

Last updated by author(s): May 25, 2022

# Reporting Summary

Nature Research wishes to improve the reproducibility of the work that we publish. This form provides structure for consistency and transparency in reporting. For further information on Nature Research policies, see our Editorial Policies and the Editorial Policy Checklist.

## Statistics

For all statistical analyses, confirm that the following items are present in the figure legend, table legend, main text, or Methods section.

| n/a | Confirmed | |
|---|---|---|
| ☐ | ☒ | The exact sample size (*n*) for each experimental group/condition, given as a discrete number and unit of measurement |
| ☐ | ☒ | A statement on whether measurements were taken from distinct samples or whether the same sample was measured repeatedly |
| ☐ | ☒ | The statistical test(s) used AND whether they are one- or two-sided<br>*Only common tests should be described solely by name; describe more complex techniques in the Methods section.* |
| ☒ | ☐ | A description of all covariates tested |
| ☒ | ☐ | A description of any assumptions or corrections, such as tests of normality and adjustment for multiple comparisons |
| ☐ | ☒ | A full description of the statistical parameters including central tendency (e.g. means) or other basic estimates (e.g. regression coefficient) AND variation (e.g. standard deviation) or associated estimates of uncertainty (e.g. confidence intervals) |
| ☐ | ☒ | For null hypothesis testing, the test statistic (e.g. *F*, *t*, *r*) with confidence intervals, effect sizes, degrees of freedom and *P* value noted<br>*Give P values as exact values whenever suitable.* |
| ☒ | ☐ | For Bayesian analysis, information on the choice of priors and Markov chain Monte Carlo settings |
| ☒ | ☐ | For hierarchical and complex designs, identification of the appropriate level for tests and full reporting of outcomes |
| ☐ | ☒ | Estimates of effect sizes (e.g. Cohen's *d*, Pearson's *r*), indicating how they were calculated |

*Our web collection on statistics for biologists contains articles on many of the points above.*

## Software and code

Policy information about availability of computer code

| | |
|---|---|
| Data collection | RT-qPCR data were acquired on a ViiA7 Real Time PCR system (Applied Biosystems, ThermoFisher Scientific). |
| Data analysis | All code used in this study for analysis of CRISPR screens can be found on Github (https://github.com/PriyankaRoy5/SARS-CoV-2-meta-analysis) and on Zenodo (DOI: 10.5281/zenodo.6499838).<br>RT-qPCR data were analyzed with QuantStudio Real-Time PCR software v1.3 (ThermoFisher Scientific). FlowJo 3 was used to analyze flow cytometry data. Excel was used to analyse the data and some of the statistical analyses, and GraphPad Prism 9 was used to represent data and for statistical analyses. |

For manuscripts utilizing custom algorithms or software that are central to the research but not yet described in published literature, software must be made available to editors and reviewers. We strongly encourage code deposition in a community repository (e.g. GitHub). See the Nature Research guidelines for submitting code & software for further information.

## Data

Policy information about availability of data

All manuscripts must include a data availability statement. This statement should provide the following information, where applicable:

- Accession codes, unique identifiers, or web links for publicly available datasets
- A list of figures that have associated raw data
- A description of any restrictions on data availability

The datasets generated during and/or analyzed during the current study have been deposited with GEO (primary screen data: GSE175666; secondary screen data: GSE193834). Additional data are available from the corresponding authors on reasonable request.
Source data are provided with this paper.

Figures 1, 2, 3 and Extended Data Figures 1, 2, 3 and 4 have associated raw data.

# Field-specific reporting

Please select the one below that is the best fit for your research. If you are not sure, read the appropriate sections before making your selection.

☒ Life sciences ☐ Behavioural & social sciences ☐ Ecological, evolutionary & environmental sciences

For a reference copy of the document with all sections, see nature.com/documents/nr-reporting-summary-flat.pdf

# Life sciences study design

All studies must disclose on these points even when the disclosure is negative.

| | |
|---|---|
| Sample size | Minimal sample sizes used in each panel has been indicated in the Figure and Extended Data Figure legends or (for the screens) in the Methods. Supplementary Data 17 spreadsheet indicates the exact number of biological repeats for each gene KO and activation sample, in all relevant figures. No statistical methods were used to predetermine sample size but sample sizes were chosen based on the approximate standard deviation generally observed from previous experiments and for a given assay. Statistical analysis data (i.e. exact p-values, when >0,0001) are provided in Supplementary Data 17. Sample sizes were sufficient to draw conclusions. |
| Data exclusions | No data were excluded from data analyses. |
| Replication | All experiments have been replicated and the minimum number of replicates is indicated in the figure legends. No experiments were included that showed contradicting results upon repetition. The main experiments were repeated at least three times to ensure reproducibility, as indicated. Supplementary Data 17 spreadsheet indicates the exact number of biological repeats for each gene KO and activation sample, in all relevant figures. |
| Randomization | The experiments in this study were not randomized in terms of sample position on experimental multiwell plates. However, experimental conditions were allocated without any previous selection of test samples (cell cultures, viral stocks, etc.) |
| Blinding | Data acquisition/analysis was merely machine based and hence blinded. |

# Reporting for specific materials, systems and methods

We require information from authors about some types of materials, experimental systems and methods used in many studies. Here, indicate whether each material, system or method listed is relevant to your study. If you are not sure if a list item applies to your research, read the appropriate section before selecting a response.

## Materials & experimental systems

| n/a | Involved in the study |
|---|---|
| ☐ | ☒ Antibodies |
| ☐ | ☒ Eukaryotic cell lines |
| ☒ | ☐ Palaeontology and archaeology |
| ☒ | ☐ Animals and other organisms |
| ☒ | ☐ Human research participants |
| ☒ | ☐ Clinical data |
| ☒ | ☐ Dual use research of concern |

## Methods

| n/a | Involved in the study |
|---|---|
| ☒ | ☐ ChIP-seq |
| ☐ | ☒ Flow cytometry |
| ☒ | ☐ MRI-based neuroimaging |

## Antibodies

Antibodies used

Primary antibodies:
- rabbit anti-ACE2 (ProteinTech 21115-1-P, lot #00086357)
- mouse anti-GAPDH-HRP (Sigma G9295, lot #107M4783V)
- mouse anti-beta Actin (Sigma-Aldrich A1978 , lot #065M4837V)
- rabbit anti-AP1B1 (ProteinTech 16932-1-AP, lot #00066081)
- rabbit anti-AP1G1 Bethyl Laboratories A304-771A, lot #1)
- rabbit anti-AAGAB (Bethyl Laboratories A305-593A, lot #2)
- mouse anti-dsRNA J2 (Scicons 10010500, lot #J2-1806)
- rabbit anti-Spike (Sino Biological Inc. 40069-T62, lot #HD11AU1103-8)
- mouse anti-VSV-G antibody (CliniSciences, clone 8G5F11, lot #T2006A22)

Secondary antibodies:
- horseradish peroxidase-conjugated anti-mouse (ThermoFisher Scientific A24512, lot #68-20-120618)
- horseradish peroxidase-conjugated anti-rabbit immunoglobulin (ThermoFisher Scientific A24537, lot #62-147-102418)

For ACE2 staining using Spike-RBD-Fc:

- Alexa-488-conjugated goat anti-mouse AlexaFluor488 antibody (ThermoFisher Scientific A10680, lot #2409037)
For the MERS-CoV immunofluorescence staining:
- Alexa-488-conjugated donkey anti-mouse IgG secondary antibody (Jackson Immunoresearch; reference 715-545-151, lot# 120989)
- Alexa594-conjugated goat anti-rabbit IgG secondary antibody (Jackson Immunoresearch; reference 111-585-144, lot# 152207)

Validation

- ACE2: https://www.ptglab.com/products/ACE2-Antibody-21115-1-AP.htm
- Actin: https://www.sigmaaldrich.com/catalog/product/sigma/a1978?lang=fr&region=FR
- GAPDH: https://www.sigmaaldrich.com/FR/fr/product/sigma/g9295?context=product
- AP1B1: https://www.ptglab.com/products/AP1B1-Antibody-16932-1-AP.htm
- AP1G1: https://www.thermofisher.com/antibody/product/gamma-Adaptin-AP1G1-Antibody-Polyclonal/A304-771A-M
- AAGAB: https://www.bethyl.com/product/A305-593A-M/AAGAB+Antibody
- dsRNA: https://www.jenabioscience.com/rna-technologies/rna-analysis-detection/dsrna-detection/rnt-sci-10010-anti-dsrna-monoclonal-antibody-j2
- VSV-G: https://www.clinisciences.com/anticorps-non-conjugues-645/mouseanti-vsv-g-8g5f11-monoclonal-447009542.html
- horseradish peroxidase-conjugated anti-mouse : https://www.thermofisher.com/antibody/product/Goat-anti-Mouse-IgG-H-L-Secondary-Antibody-Polyclonal/A24512
- horseradish peroxidase-conjugated anti-rabbit immunoglobulin : https://www.thermofisher.com/antibody/product/Goat-anti-Rabbit-IgG-H-L-Cross-Adsorbed-Secondary-Antibody-Polyclonal/A24537
- Alexa-488-conjugated goat anti-mouse antibody (for staining using Spike-RBD-Fc): https://www.thermofisher.com/antibody/product/Goat-anti-Mouse-IgG-IgM-H-L-Secondary-Antibody-Polyclonal/A-10680
For the MERS-CoV immunofluorescence staining:
- Alexa-488-conjugated donkey anti-mouse IgG secondary antibody : https://www.jacksonimmuno.com/catalog/products/715-545-151
- Alexa594-conjugated goat anti-rabbit IgG secondary antibody : https://www.jacksonimmuno.com/catalog/products/111-585-144

## Eukaryotic cell lines

Policy information about cell lines

Cell line source(s)

Caco-2 (ATCC HTB-37)
Calu-3 (ATCC HTB-55)
LLC-MK2 (ATCC CCL7.1)
Vero E6 (Sigma Aldrich N°85020205)
A549 (ATCC CCL-185)
HEK293T (ATCC CRL-3216)
MDCK (ATCC CCL-34)
Huh7 were described in reference Nakabayashi, H., Taketa, K., Miyano, K., Yamane, T. & Sato, J. Growth of human hepatoma cells lines with differentiated functions in chemically defined medium. Cancer Res 42, 3858–3863 (1982).
Huh7.5.1 were described in reference Zhong, J. et al. Robust hepatitis C virus infection in vitro. Proc Natl Acad Sci U S A 102, 9294–9299 (2005).

Authentication

Cell lines were not independently authenticated (with the exception of Huh7 cells, which have been authenticated by Multiplexion company, by SNPtyping). However, large frozen stocks of each cell line were generated as soon as possible following their receival and new batches from frozen aliquots are regularly thawed.

Mycoplasma contamination

All cell lines tested were routinely tested for mycoplasma infection using Lonza MycoAlert detection kit and were negative.

Commonly misidentified lines
(See ICLAC register)

No commonly misidentified lines were used in this study.

## Flow Cytometry

### Plots

Confirm that:

☒ The axis labels state the marker and fluorochrome used (e.g. CD4-FITC).

☒ The axis scales are clearly visible. Include numbers along axes only for bottom left plot of group (a 'group' is an analysis of identical markers).

☒ All plots are contour plots with outliers or pseudocolor plots.

☒ A numerical value for number of cells or percentage (with statistics) is provided.

### Methodology

Sample preparation

For mNG reporter analysis, cells were trypsinized and fixed prior to flow cytometry analysis. For ACE2 staining using Spike-RBD-Fc, cells were detached using PBS-EDTA and stained as described in the Methods.

Instrument

Data collection was done on a NovoCyte (ACEA Biosciences Inc.)

| | |
|---|---|
| Software | Flow cytometry data were analyzed using FlowJo (3 or higher). |
| Cell population abundance | At least 5,000 events were acquired within the gated population to analyse mNG expression and ACE2 staining. |
| Gating strategy | FSC-A/SSC-A parameters were used to gate the cells and the negative control population (i.e. non-infected cells) was used to set the fluorescent positive gate (as shown in Extended Data Figure 5a). |

☒ Tick this box to confirm that a figure exemplifying the gating strategy is provided in the Supplementary Information.